© 2014. Published by The Company of Biologists Ltd | Development (2014) 141, 4182-4193 doi:10.1242/dev.111260

RESEARCH ARTICLE

The tumor suppressor Nf2 regulates corpus callosum development by inhibiting the transcriptional coactivator Yap

Alfonso Lavado, Michelle Ware*,‡, Joshua Paré‡ and Xinwei Cao§

ABSTRACT

The corpus callosum connects cerebral hemispheres and is the largest axon tract in the mammalian brain. Callosal malformations are among the most common congenital brain anomalies and are associated with a wide range of neuropsychological deficits. Crossing of the midline by callosal axons relies on a proper midline environment that harbors guidepost cells emitting guidance cues to instruct callosal axon navigation. Little is known about what controls the formation of the midline environment. We find that two components of the Hippo pathway, the tumor suppressor Nf2 (Merlin) and the transcriptional coactivator Yap (Yap1), regulate guidepost development and expression of the guidance cue Slit2 in mouse. During normal brain development, Nf2 suppresses Yap activity in neural progenitor cells to promote guidepost cell differentiation and prevent ectopic Slit2 expression. Loss of Nf2 causes malformation of midline guideposts and Slit2 upregulation, resulting in callosal agenesis. *Slit2* heterozygosity and *Yap* deletion both restore callosal formation in *Nf2* mutants. Furthermore, selectively elevating Yap activity in midline neural progenitors is sufficient to disrupt guidepost formation, upregulate Slit2 and prevent midline crossing. The Hippo pathway is known for its role in controlling organ growth and tumorigenesis. Our study identifies a novel role of this pathway in axon guidance. Moreover, by linking axon pathfinding and neural progenitor behaviors, our results provide an example of the intricate coordination between growth and wiring during brain development.

KEY WORDS: Commissure, Radial glia, Glial wedge, Indusium griseum, Guidepost neurons, Nervous system

INTRODUCTION

The corpus callosum is the largest commissural axon tract in the mammalian brain. It transfers sensory, motor and cognitive information between cerebral hemispheres. An innovation during eutherian evolution, the corpus callosum is believed to be involved in higher order brain functions. Callosal malformations are among the most common congenital brain anomalies and are associated with cognitive, behavioral and neurological deficits (Paul et al., 2007).

Callosal formation requires a cascade of dynamic events to be precisely coordinated spatially and temporally (Donahoo and Richards, 2009; Fame et al., 2011; Nishikimi et al., 2013). Callosal projection neurons mainly reside in cortical layers II and III and, to a lesser extent, layers V and VI. In the mouse, axons from the cingulate cortex approach and cross the midline first at around embryonic day (E) 16 and are later joined by axons from the neocortex (Koester and O'Leary, 1994; Rash and Richards, 2001). To reach their targets in the contralateral hemisphere, callosal axons follow the guidance cues emitted by several glial and neuronal guidepost structures at the corticoseptal boundary region. Defects in callosal neuron specification and production, midline patterning, guidepost formation or guidance cue expression and reception might result in complete or partial agenesis of the corpus callosum. Although it has long been recognized that the environment which callosal axons traverse is crucial for their pathfinding, how this environment is shaped is not well understood. Despite recent progress (Amaniti et al., 2013; Benadiba et al., 2012; Chinn et al., 2014; Magnani et al., 2014; Piper et al., 2009a; Shu et al., 2003a,b; Smith et al., 2006; Unni et al., 2012), our knowledge of what regulates the development of guideposts and expression of guidance molecules remains limited.

Neurofibromatosis type 2 is an inherited syndrome in which individuals develop nervous system tumors (Li et al., 2012). It is caused by inactivating mutations of the neurofibromatosis 2 (*NF2*) tumor suppressor gene, which encodes a Four-point-one, Ezrin, Radixin, Moesin (FERM) domain-containing protein that is also known as Merlin. Nf2 (Merlin) is widely expressed and engages in many signaling pathways, including the Rac-PAK, mTORC1, EGFR, PI3K-Akt and Hippo pathways. It regulates diverse cellular processes, such as the establishment of cell polarity, formation of cell-cell junctions and proliferation. Nf2 plays numerous roles in the nervous system, including promoting cell-cell adhesion during neural tube closure (McLaughlin et al., 2007), inhibiting glial cell proliferation (Giovannini et al., 2000; Houshmandi et al., 2009) and maintaining axonal integrity (Schulz et al., 2013).

Using *Nf2* conditional knockout mouse models, we have previously shown that Nf2 limits the expansion of neural progenitor cell (NPC) populations during brain development by inhibiting the transcriptional coactivators Yap (Yap1 – Mouse Genome Informatics) and its paralog Taz (here referred to as Yap/Taz) (Lavado et al., 2013). Nf2 loss and YAP hyperactivation also render the dentate gyrus radial glial scaffold over-exuberant and impair hippocampus morphogenesis. We unexpectedly discovered that *Nf2* mutants lack the corpus callosum. However, it was unclear mechanistically how Nf2 regulates callosal development.

Here, we investigate the underlying cellular and molecular basis for the role of Nf2 in callosal development. We find that Nf2 is not required in callosal neurons or their progenitors in order for the corpus callosum to form, but it is required in midline NPCs for proper formation of the midline environment that callosal axons encounter. We further demonstrate that Nf2 functions by suppressing Yap, which in turn regulates guidepost development and expression of the guidance cue Slit2. Our study uncovers the mechanistic basis of how the tumor suppressor Nf2 regulates callosal formation and provides novel insights into the molecular mechanisms that shape the callosal midline environment.

Department of Developmental Neurobiology, St. Jude Children's Research Hospital, Memphis, TN 38105, USA.
*Present address: Institut de Génétique et Développement de Rennes, France.
‡These authors contributed equally to this work

§Author for correspondence (Xinwei.cao@stjude.org)

Received 10 April 2014; Accepted 1 September 2014

Development (2014) 141, 4182-4193 doi:10.1242/dev.111260

RESULTS

Nf2 is required for corpus callosum and hippocampal commissure development

We previously found that deleting floxed alleles of *Nf2* ($Nf2^{F/F}$) (Giovannini et al., 2000) with *Emx1-cre*, which is expressed in the dorsal telencephalon by E10.5 (Gorski et al., 2002), results in callosal agenesis (Lavado et al., 2013). Luxol Blue staining of adult brain sections to detect myelinated axons showed that, in *Nf2* mutants ($Nf2^{F/F}$;*Emx1-Cre*), the corpus callosum was absent along the rostrocaudal axis with few, if any, fibers crossing the midline (Fig. 1A-D, arrow). The hippocampal commissure was also lacking (Fig. 1E,F, arrow), whereas the anterior commissure formed normally (Fig. 1C,D, arrowhead). The acallosal phenotype was never observed in $Nf2^{F/+}$;*Emx1-Cre* animals, suggesting that the defect was not due to strain background. Deleting *Nf2* using *Nestin-Cre* (Tronche et al., 1999), which is expressed in NPCs throughout the central nervous system, also led to agenesis of the corpus callosum and hippocampal commissure (supplementary material Fig. S1). Here, we focused on understanding the role of Nf2 in callosal development.

Nf2 transcripts have been detected in NPCs and cortical neurons during mouse brain development (McLaughlin et al., 2007). We examined Nf2 protein localization at E15.5, when pioneer axons reach the midline. As reported previously (Lavado et al., 2013), Nf2 localized at the apical region of NPCs, highlighting the ventricular surface (Fig. 1G, arrowhead). Nf2 was also detected in the cortical plate (Fig. 1G, dashed bracket) and in axons reaching the midline (Fig. 1G, arrow). Co-staining with an antibody against L1 cell adhesion molecule (L1), which labels axons, confirmed that Nf2 was present in callosal axons (Fig. 1G′, arrow). All Nf2 immunoreactivity in the dorsal telencephalon was eliminated in $Nf2^{F/F}$;*Emx1-Cre* embryos (Fig. 1H,H′), indicating that the observed signals were specific. Thus, Nf2 is expressed in callosal neurons and the NPCs that give rise to callosal neurons and midline structures. This expression pattern suggests that the acallosal phenotype caused by loss of Nf2 might arise from (1) defects in callosal neurons, including their specification, production and ability to project axons and respond to guidance cues, or (2) defects in the environment that callosal axons encounter, including midline patterning, guidepost formation and the expression of guidance cues. We investigated all of these possibilities.

A defective midline is responsible for callosal agenesis in *Nf2* mutants

First we examined whether callosal neurons were generated properly in *Nf2* mutants. The expression patterns of Satb2, a transcription factor required for callosal neuron specification (Alcamo et al., 2008; Britanova et al., 2008), and cortical layer-specific markers Ctip2 (layers V and VI) and Tbr1 (layers II, III, V and VI) were normal in *Nf2* mutants at E15.5 and E17.5 (supplementary material Fig. S2), demonstrating that callosal neuron production and cortical laminar organization are largely unperturbed upon *Nf2* deletion.

To determine whether Nf2 is required in callosal neurons for callosal formation, we specifically deleted *Nf2* in callosal neurons using a *Satb2-Cre* line. Using the Cre-reporter line *Rosa-CAG-LSL-tdTomato* (*R26R-tdTomato*) (Madisen et al., 2010), which expresses tdTomato upon Cre-mediated deletion of the *LoxP-Stop-LoxP* (*LSL*) cassette, we confirmed that Cre activity was turned on at around E13.5 and was mostly restricted to callosal neurons (supplementary

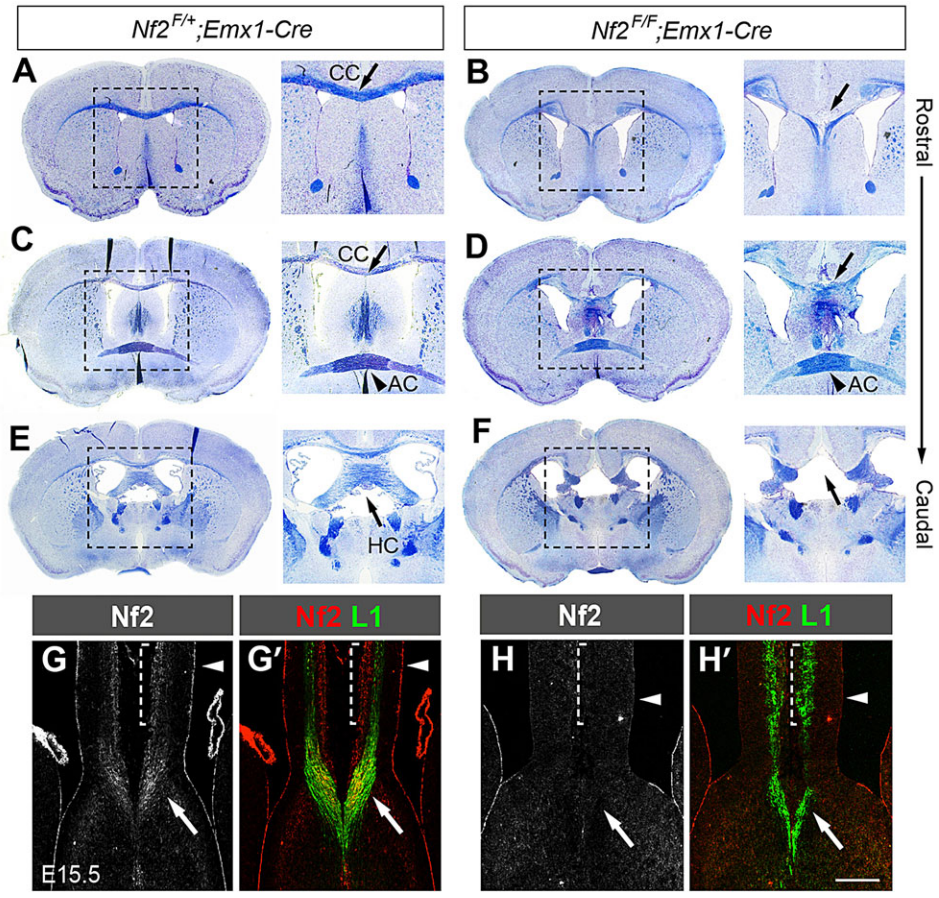

Fig. 1. Agenesis of the corpus callosum and hippocampal commissure in *Nf2* mutants. (A-F) Luxol Blue staining of myelinated axons (blue) and Cresyl Violet staining of cell bodies (purple) showing agenesis of the corpus callosum (CC) (A-D, arrow) and hippocampal commissure (HC) (E,F, arrow) but normal anterior commissure (AC) (C,D, arrowhead) in 2-month-old $Nf2^{F/F}$;*Emx1-Cre* mice (n=3). A magnified view of the boxed region is shown in the image to the right. (G,G′) Immunostaining showing Nf2 localization at the ventricular surface (arrowhead), cortical plate (dashed bracket) and $L1^+$ callosal axons (arrow) in control brains at E15.5. (H,H′) Nf2 immunoreactivity in these regions is eliminated in $Nf2^{F/F}$;*Emx1-Cre* dorsal telencephalon. Arrowhead, ventricular surface; arrow, callosal axons. Scale bar: 200 µm.

Development (2014) 141, 4182-4193 doi:10.1242/dev.111260

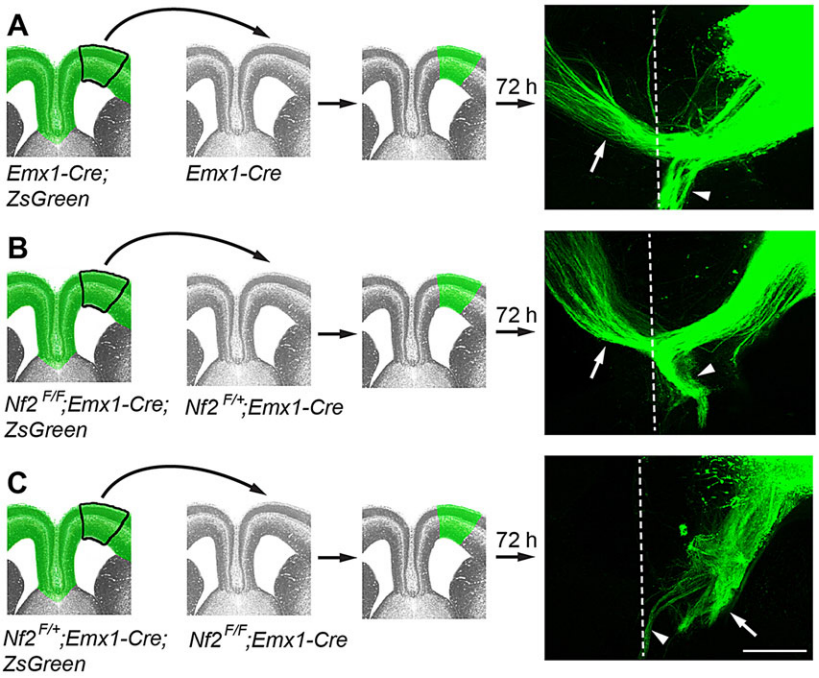

Fig. 2. Callosal axons from *Nf2* mutant brains can cross the midline of control forebrains. Tissues from the frontal cortex of E16.5 ZsGreen^{+} donor embryos were transplanted into cortical sections of ZsGreen^{-} host embryos and then cultured for 72 h. Axon trajectory was examined using ZsGreen fluorescence. Panels show transplantation schemes with the genotypes of donor and host embryos indicated, and examples of transplants are shown on the right. Dashed line, the midline; white arrow, callosal axons; arrowhead, mis-projected axons. (A) Control callosal axons cross the midline of control hosts. (B) Callosal axons from *Nf2*$^{F/F}$;*Emx1-Cre* embryos cross the midline of *Nf2*$^{F/+}$;*Emx1-Cre* hosts. (C) Callosal axons from *Nf2*$^{F/+}$;*Emx1-Cre* embryos fail to cross the midline of *Nf2*$^{F/F}$;*Emx1-Cre* hosts. Scale bar: 200 µm.

material Fig. S3A-C). No Cre activity was detected in progenitor cells at the ventricular zone and subventricular zone (supplementary material Fig. S3A,B). In E15.5 *Nf2*$^{F/F}$;*Satb2-Cre* embryos, Nf2 immunoreactivity was preserved at the ventricular surface (supplementary material Fig. S3D-E′, arrowhead) but lost in callosal axons (supplementary material Fig. S3D-E′, arrow). The corpus callosum formed normally in these mutants (supplementary material Fig. S3F,G), suggesting that Nf2 is not required in callosal neurons for callosal formation.

To further test whether *Nf2*-deficient callosal neurons were able to project axons across the midline, we performed *ex vivo* transplantation experiments. We introduced a Cre-reporter gene, *Rosa-CAG-LSL-ZsGreen* (*ZsGreen*) (Madisen et al., 2010), into the *Nf2*$^{F/F}$ background to visualize axons. In control experiments, homotopic transplantation of the frontal cortex of *Emx1-Cre*; *ZsGreen* embryos at E16.5 into cortical sections of *Emx1-Cre* hosts resulted in midline crossing of ZsGreen^{+} callosal axons after 72 h in culture (n=7 out of 7; Fig. 2A, white arrow). Axons from *Nf2* mutant (*Nf2*$^{F/F}$;*Emx1-Cre*;*ZsGreen*) cortices were also able to cross the midline of *Nf2*$^{F/+}$;*Emx1-Cre* hosts (n=5 out of 5; Fig. 2B, white arrow). By contrast, axons from *Nf2*$^{F/+}$;*Emx1-Cre*;*ZsGreen* cortices failed to cross the midline of *Nf2* mutant hosts (n=0 out of 10; Fig. 2C, white arrow). We often observed that, in all three transplantation scenarios, some axons mis-projected ventrally into the septum (Fig. 2A-C, arrowheads). This is probably an artifact caused by, for example, imperfect sectioning or grafting. Nevertheless, the stark contrast between *Nf2* mutant axons being able to cross the midline of control hosts (Fig. 2B) and control axons unable to cross the midline of *Nf2* mutant hosts (Fig. 2C) strongly suggests that Nf2 is not required for the production of callosal neurons capable of projecting axons across the midline, but is required to generate the midline environment.

Nf2 is required for glial wedge development

Upon determining that midline defects are responsible for callosal agenesis in *Nf2* mutants, we first examined early patterning at the corticoseptal boundary where midline guideposts later form. At E12.5 and E15.5, the expression patterns of Six3, Zic2 and Nfia, transcription factors delineating subdomains of the commissural plate (Moldrich et al., 2010), were unaffected upon *Nf2* deletion (supplementary material Fig. S4A-F′). Gli3 and Fgf8 are required for corticoseptal boundary patterning and callosal formation (Amaniti et al., 2013; Magnani et al., 2014; Moldrich et al., 2010). Their expression and that of *Sprouty1*, a target of Fgf signaling, appeared normal in *Nf2* mutants (supplementary material Fig. S4A-D′,G-J′). Interestingly, quantitative western blot analyses of Gli3 using E13.5 cortex and E15.5 medial-cortex tissues showed that the amounts of the full-length activator form (Gli3FL) and cleaved repressor form (Gli3R) and the ratio of Gli3FL to Gi3R were increased in *Nf2* mutants (supplementary material Fig. S5), although the functional consequence of these changes is unclear. *Wnt8b* and the Wnt target gene *Axin2* were expressed normally in *Nf2* mutants except for an elongation of the *Wnt8b*$^{+}$ domain at E15.5 (supplementary material Fig. S4K-N′), which correlated with the elongation of the glial wedge (see below, Fig. 3A-B′). *Axin2 in situ* hybridization signals were very weak at E15.5 (supplementary material Fig. S4N,N′). We performed quantitative RT-PCR (qRT-PCR) analysis using rostral medial-cortex tissues at E15.5, which also showed similar *Axin2* mRNA levels in control and *Nf2* mutants (n=3 embryos per genotype, P=0.8). Taken together, these results suggest that patterning of the corticoseptal boundary is grossly normal in *Nf2* mutants.

Next we examined the development of midline guideposts between E15.5 and E17.5, before and during callosal formation. The glial wedge (GW) is located at the ventricular zone on either side of the midline and deflects callosal axons toward the midline (Shu and Richards, 2001). At these stages, the GW is composed of NPCs, which are also known as radial glia (Kriegstein and Alvarez-Buylla, 2009; Shu et al., 2003b; Smith et al., 2006). GW cells initially extend long GFAP^{+} radial processes to the midline pia, but lose their pial attachment by E15.5, when pioneer axons reach the midline (Shu et al., 2003b) (Fig. 3A,A′, arrowhead). In *Nf2* mutants, the GW was formed but dorsoventrally spanned a broader region than that in controls (Fig. 3A-B′, white line). Moreover, many

Development (2014) 141, 4182-4193 doi:10.1242/dev.111260

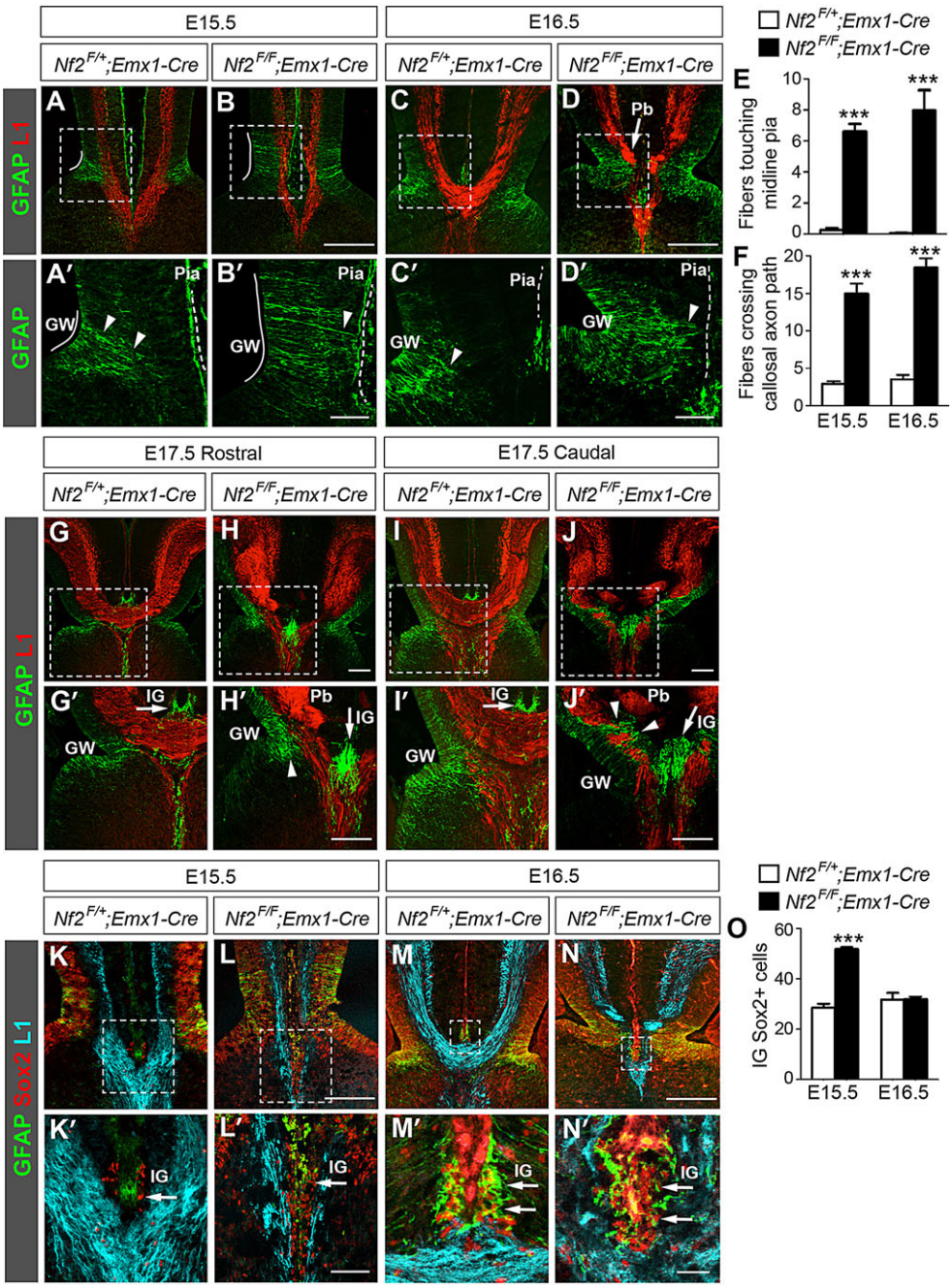

Fig. 3. Nf2 loss impairs glial wedge development. (A,A′) In control embryos at E15.5, GFAP$^+$ processes (arrowhead) from the glial wedge (GW, white line) have detached from the pia (dashed line). At this stage, the GFAP antibody often stains the pia nonspecifically. Panels labeled with primes are the magnified view of the boxed areas in corresponding panels. (B,B′) In *Nf2$^{F/F}$;Emx1-Cre* embryos, the GW is elongated and many GW processes remain attached to the pia and intersect L1$^+$ callosal axons (B′, arrowhead). (C-D′) In E16.5 *Nf2$^{F/F}$;Emx1-Cre* embryos, GW fibers still extend close to the pia (D′, arrowhead) and Probst bundles (Pb) are formed (D, arrow). (E,F) More GFAP$^+$ GW fibers touch the midline pia (E, *n*=4) and more cross callosal axon path (F, *n*=6) in *Nf2$^{F/F}$;Emx1-Cre* embryos than in controls. ***P<0.001. (G-J′) In E17.5 *Nf2$^{F/F}$;Emx1-Cre* brains, GW fibers have lost pial attachment in rostral regions (H′, arrowhead) but still project close to the pia and intersect axons of the corpus callosum or hippocampal commissure in caudal regions (J′, arrowhead). Arrow: indusium griseum (IG). (K-L′) At E15.5, Sox2$^+$ cells are present in the IG primordium in control and *Nf2$^{F/F}$;Emx1-Cre* embryos (arrow). These cells are GFAP$^-$ at this stage. (M-N′) GFAP$^+$ IG astrocytes (arrow) are present in control and *Nf2$^{F/F}$;Emx1-Cre* embryos at E16.5. Most of these cells also express Sox2. (O) The number of IG Sox2$^+$ cells is increased in *Nf2$^{F/F}$;Emx1-Cre* embryos at E15.5 (*n*=5) but is similar to that in controls at E16.5 (*n*=4). Scale bars: 200 µm in B,D,H,H′,J,J′,L,N; 50 µm in B′,D′,L′; 10 µm in N′.

GFAP$^+$ processes remained attached to the midline pia, crossing the path of callosal axons (Fig. 3B,B′, arrowhead; Fig. 3E,F). At E16.5, when many callosal axons have crossed the midline in controls (Fig. 3C), some GW fibers in *Nf2* mutants still extended close to the pia (Fig. 3D,D′, arrowhead; Fig. 3E,F) and callosal axons, failing to cross the midline, accumulated into abnormal tangles known as Probst bundles (Fig. 3D, arrow). By E17.5, GW fibers in *Nf2* mutants no longer projected close to the pia in rostral regions (Fig. 3H,H′, arrowhead), but still transected the path of callosal or hippocampal commissural axons in caudal regions (Fig. 3J,J′, arrowhead). Thus, GW formation was perturbed in *Nf2* mutants, manifesting as elongation of the GW region and overextension of radial processes.

The indusium griseum (IG) comprises neurons and astrocytes underneath the midline pia, above the corpus callosum. Because IG astrocytes do not express GFAP until E17 (Shu et al., 2003b), we searched for other IG markers to examine the earlier stages of its development. At E15.5, at least a fraction of cells beneath the midline pia expressed Sox2 (Fig. 3K,K′, arrow) and some Sox2$^+$ cells were also immunopositive for GFAP at E16.5 (Fig. 3M,M′, arrow), suggesting that Sox2 is an earlier marker for IG cells. The immunostaining pattern of Sox2 overlapped with that of Sox9 (supplementary material Fig. S6A-B′), another IG glia marker (Clegg et al., 2014). Similar to controls, Sox2$^+$, GFAP$^+$ and Sox9$^+$ cells were present beneath the midline pia in *Nf2* mutants from E15.5 to E17.5 (Fig. 3K-N′,G-J′, arrows; supplementary material Fig. S6C-F′). We noted that the numbers of Sox2$^+$ cells and Sox9$^+$ cells were increased in *Nf2* mutants at E15.5 but returned to control levels at E16.5 (Fig. 3O; supplementary material Fig. S6G). The functional significance of this change is unclear. We also noticed

Development (2014) 141, 4182-4193 doi:10.1242/dev.111260

that the IG in *Nf2* mutants was mis-positioned at the same dorsoventral level as the GW, instead of dorsal to it as in controls (Fig. 3G-J′). This defect, however, might be secondary to the lack of crossing callosal axons. Taken together, we conclude that IG development is largely unaffected in *Nf2* mutants, except for a transient increase in IG glia at E15.5.

Nf2 promotes differentiation of glutamatergic guidepost neurons

Next we investigated the development of midline guidepost neurons, which comprise GABAergic interneurons and Calretinin-positive glutamatergic neurons and attract callosal axons (Niquille et al., 2009). Because GABAergic neurons are produced by NPCs at the ventral telencephalon (Niquille et al., 2009), *Nf2* deletion using *Emx1-Cre* is unlikely to directly affect GABAergic neurons. We therefore focused on Calretinin$^+$ glutamatergic neurons. At E15.5, these neurons resided at the midline cortical plate, forming a band between the pia and GW processes (Fig. 4A,A′). In *Nf2* mutants, Calretinin$^+$ neurons were significantly reduced [310±4 per section in controls versus 225±4 (mean±s.e.m.) in *Nf2* mutants, n=4, P<0.0001], and the band of these cells was bisected by a gap (Fig. 4B,B′, arrowhead). This gap coincided precisely with the GW fibers that remained attached to the pia (Fig. 4B′, arrowheads) and was occupied by Tbr2$^+$ intermediate progenitors (Fig. 4D,D′, arrowheads), which normally reside at the subventricular zone (Fig. 4C,C′). The presence of Tbr2$^+$ cells in the cortical plate indicated that differentiation of Calretinin$^+$ neurons might be affected. To test this, we performed birth-dating experiments. We injected BrdU into pregnant mice at E13.5 to label S-phase progenitor cells. Two days later, many BrdU-labeled cells in controls had differentiated into Calretinin$^+$ neurons (Fig. 4E,E′, yellow cells, arrowheads). In *Nf2* mutants, BrdU-labeled cells predominantly remained as Tbr2$^+$ intermediate progenitors or ventricular zone NPCs, and significantly fewer of them differentiated into Calretinin$^+$ neurons (Fig. 4F,F′; 84±9 BrdU$^+$Calretinin$^+$ neurons per section in controls versus 33±2 in *Nf2* mutants, n=3, P=0.0056). These results demonstrate that Nf2 promotes differentiation of Calretinin$^+$ guidepost neurons.

Upregulation of *Slit2* contributes to callosal agenesis in *Nf2* mutants

Next, we examined whether *Nf2* deletion affects the expression of guidance molecules that are important for callosal formation. Similar to E15.5-16.5 controls, callosal axons in *Nf2* mutants were immunopositive for guidance receptors Neuropilin-1 (Piper et al., 2009b) and Dcc (Fazeli et al., 1997), and *Robo1* (Andrews et al., 2006) transcripts were detected in the cell bodies of cingulate neurons (supplementary material Fig. S7A-F). Midline guidance cues Sema3c (Niquille et al., 2009; Piper et al., 2009b), Netrin1 (Serafini et al., 1996) and Draxin (Islam et al., 2009) were expressed normally in *Nf2* mutants (supplementary material Fig. S7G-L). *Robo1*, *Sema3c* and *Netrin1* transcripts are usually present in the region where Calretinin$^+$ neurons reside (supplementary material Fig. S7E,G,I, dashed bracket). In *Nf2* mutants, the apparent lack or downregulation of these transcripts in that region is probably due to fewer Calretinin$^+$ neurons (see Fig. 4) rather than to reduced transcription. Interestingly, *Slit2*, which is expressed in the midline ventricular zone at E15.5 and is required for callosal formation (Bagri et al., 2002; Shu and Richards, 2001), was induced in *Nf2* mutants (Fig. 5A,B). To confirm the change in the level of *Slit2*, we performed qRT-PCR analysis using E14.5 medial-cortex tissues. The *Slit2* mRNA level was increased 1.7±0.1 fold in *Nf2* mutants (n=3, P=0.0087).

Previous *in vitro* assays show that Slit2 repels cortical axons (Shu and Richards, 2001). To test whether *Slit2* upregulation in *Nf2*

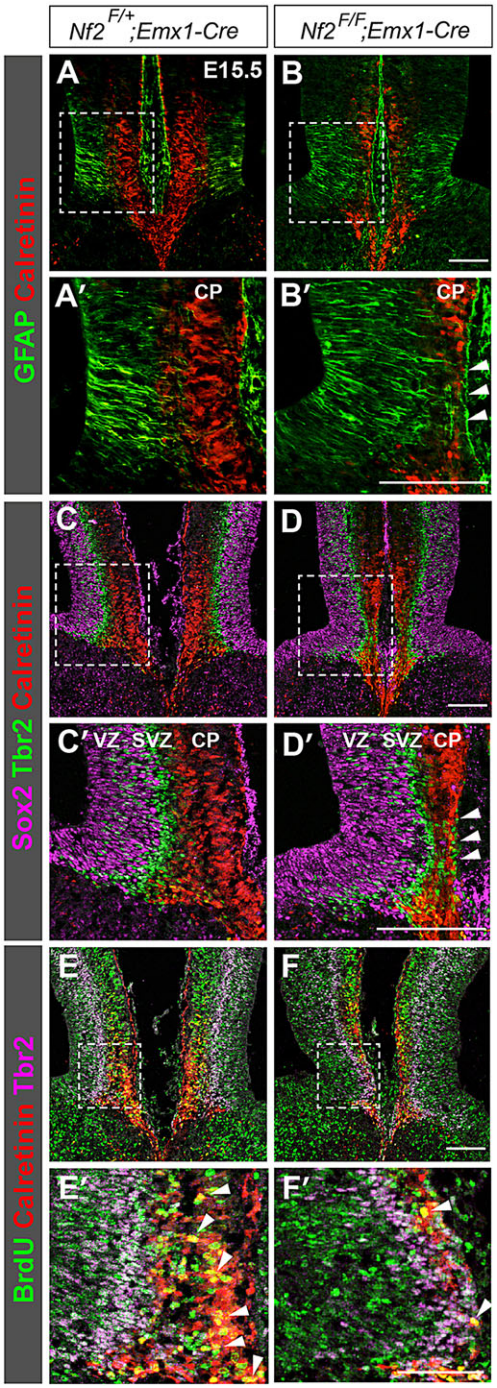

Fig. 4. Loss of *Nf2* reduces glutamatergic guidepost neurons. (A,A′) In control embryos at E15.5, Calretinin$^+$ guidepost neurons reside at the midline cortical plate (CP). (B,B′) Fewer Calretinin$^+$ neurons are found in *Nf2$^{F/F}$;Emx1-Cre* midline, especially at the region where GW fibers remain attached to the pia (B′, arrowhead). (C,C′) In controls, Sox2$^+$ neural progenitor cells (NPCs), Tbr2$^+$ intermediate progenitors and Calretinin$^+$ neurons reside at the ventricular zone (VZ), subventricular zone (SVZ) and CP, respectively. (D,D′) In the midline of *Nf2$^{F/F}$;Emx1-Cre* mice, Tbr2$^+$ intermediate progenitors intermingle with Calretinin$^+$ neurons (arrowheads). (E-F′) BrdU was administered at E13.5, and embryos were harvested 48 h later. Many BrdU-labeled cells in controls are Calretinin$^+$ (E,E′, yellow cells, arrowhead). In *Nf2$^{F/F}$;Emx1-Cre* embryos, most BrdU-labeled cells remain as VZ NPCs or Tbr2$^+$ intermediate progenitors (F,F′) and fewer of them have differentiated into Calretinin$^+$ neurons (F′, yellow cells, arrowheads). Panels labelled with primes are the magnified view of the boxed areas in corresponding panels. Scale bars: 100 µm.

Development (2014) 141, 4182-4193 doi:10.1242/dev.111260

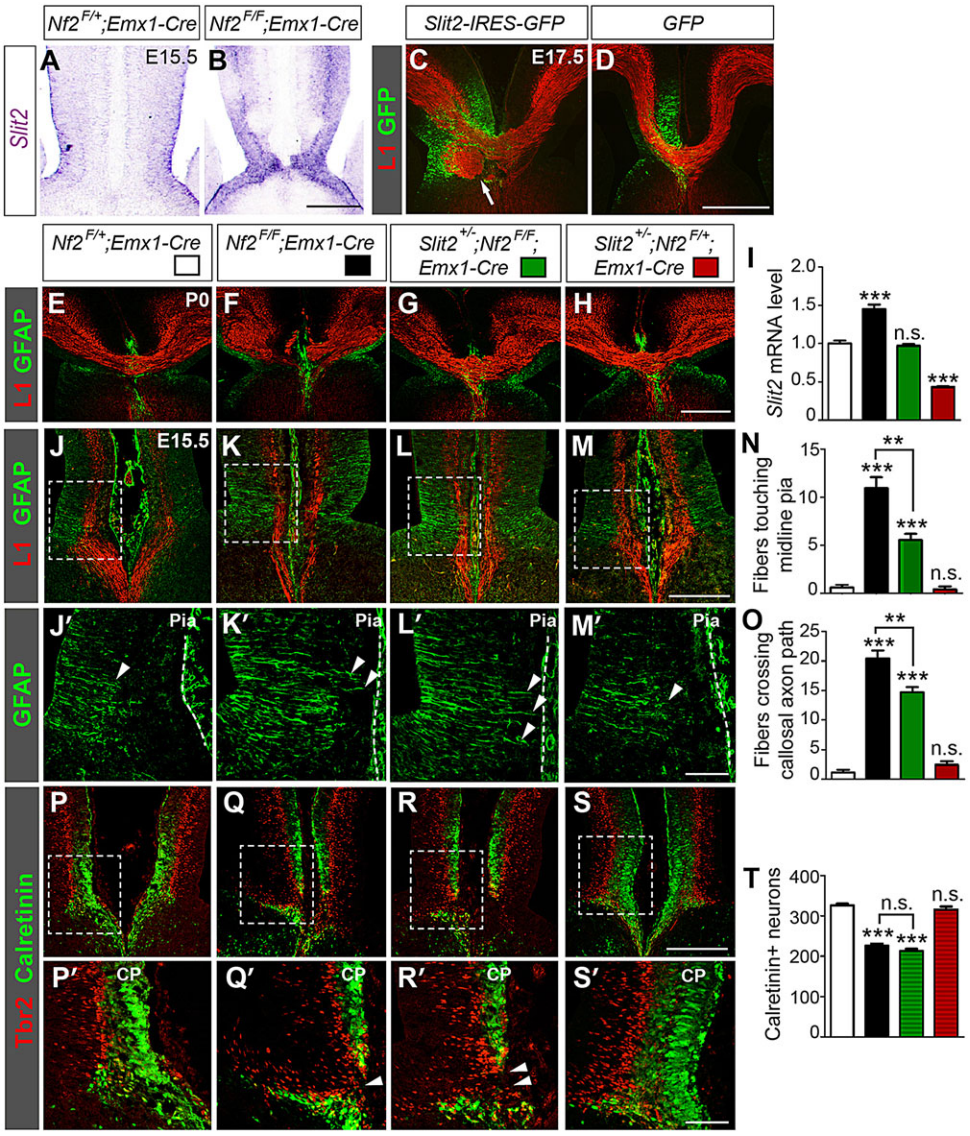

Fig. 5. *Slit2* upregulation contributes to callosal agenesis in *Nf2* mutants. (A,B) *In situ* hybridization shows higher *Slit2* levels in E15.5 $Nf2^{F/F}$;*Emx1-Cre* midline than in control. (C,D) Overexpressing *Slit2* by using *in utero* electroporation at E13.5 results in formation of axon tangles at E17.5 (C, arrow). GFP overexpression does not cause this defect (D). (E-H) Sections of littermates show that *Slit2* heterozygosity in the $Nf2^{F/F}$;*Emx1-Cre* background restores the corpus callosum (G). (I) qRT-PCR analyses of E15.5 rostral medial-cortex tissues show that although the *Slit2* mRNA level is upregulated in $Nf2^{F/F}$;*Emx1-Cre* embryos, it is returned to control ($Nf2^{F/+}$;*Emx1-Cre*) levels in $Slit2^{+/-}$;$Nf2^{F/F}$;*Emx1-Cre* embryos (n=4). (J-O) *Slit2* heterozygosity does not fully rescue the GW defects of *Nf2* mutants. More GFAP$^+$ GW fibers (arrowheads) touch the midline pia (dashed line) and more cross the callosal axon path in $Slit2^{+/-}$;$Nf2^{F/F}$;*Emx1-Cre* embryos than in littermate $Nf2^{F/+}$;*Emx1-Cre* controls. These defects are similar to those in $Nf2^{F/F}$;*Emx1-Cre* embryos, albeit less severe. $Slit2^{+/-}$;$Nf2^{F/+}$;*Emx1-Cre*, n=3; the rest, n=5. (P-T) Calretinin$^+$ neurons are reduced in $Slit2^{+/-}$;$Nf2^{F/F}$;*Emx1-Cre* embryos compared to that in $Nf2^{F/+}$;*Emx1-Cre* controls and Tbr2$^+$ intermediate progenitors are present in the midline cortical plate (CP) (arrowheads). These defects are similar to those in $Nf2^{F/F}$;*Emx1-Cre* embryos. $Slit2^{+/-}$;$Nf2^{F/+}$;*Emx1-Cre*, n=3; the rest, n=4. Scale bars: 200 µm (B,M, S); 500 µm (D,H); 50 µm (M′,S′). Panels labeled with primes are magnified views of the boxed areas in corresponding panels. In panels I,N,O,T, statistical significance scores are evaluated against $Nf2^{F/+}$;*Emx1-Cre* embryos unless specifically indicated. **P<0.01; ***P<0.001; n.s., not significant.

mutants contributes to callosal agenesis, we overexpressed Slit2 *in vivo* at the corticoseptal boundary by performing *in utero* electroporation at E13.5. At E17.5, Slit2 overexpression resulted in the accumulation of abnormal axon tangles in the side that had been transfected (n=4 out of 4; Fig. 5C, arrow), although it did not prevent callosal formation. Axon tangles were never observed after overexpression of green fluorescent protein (GFP) (n=0 out of 4, Fig. 5D). These results suggest that *Slit2* upregulation could contribute to callosal agenesis in *Nf2* mutants.

To further confirm the involvement of *Slit2* upregulation, we tested whether deleting *Slit2* in *Nf2* mutants suppresses the acallosal phenotype. Remarkably, deleting one allele of *Slit2* fully restored the corpus callosum in neonatal (P0) *Nf2* mutants (n=5 out of 5, Fig. 5G), whereas it had no discernible effect in the *Nf2* heterozygous background (Fig. 5H). qRT-PCR analysis of E15.5 rostral medial-cortex tissues showed that although the *Slit2* mRNA level was increased in $Nf2^{F/F}$;*Emx1-Cre* embryos, it was returned to littermate control ($Nf2^{F/+}$;*Emx1-Cre*) levels in $Slit2^{+/-}$;$Nf2^{F/F}$;*Emx1-Cre* embryos (Fig. 5I). *Slit2* heterozygosity, however, did not fully rescue guidepost development. In $Slit2^{+/-}$;$Nf2^{F/F}$;*Emx1-Cre* embryos, more GFAP$^+$ GW processes extended close to the pia than those in littermate controls ($Nf2^{F/+}$;*Emx1-Cre* and $Slit2^{+/-}$;$Nf2^{F/+}$;*Emx1-Cre*) (Fig. 5J-O, arrowheads), although the defects were not as severe as they were in $Nf2^{F/F}$;*Emx1-Cre* embryos. Fewer Calretinin$^+$ guidepost neurons were found in $Slit2^{+/-}$;$Nf2^{F/F}$;*Emx1-Cre* embryos than in controls (Fig. 5P-T), and the bands of Calretinin$^+$ neurons were interrupted by Tbr2$^+$ intermediate progenitors (Fig. 5R,R′, arrowhead), again resembling the phenotypes of $Nf2^{F/F}$;*Emx1-Cre* embryos. Taken together, these results suggest that *Slit2* upregulation contributes to callosal agenesis in *Nf2* mutants.

Yap overactivation is responsible for callosal agenesis in *Nf2* mutants

Next, we sought to understand how *Nf2* deletion leads to guidepost malformation and *Slit2* upregulation. Two lines of evidence suggested that overactivation of the Yap/Taz transcriptional coactivators might be responsible. First, we have previously shown that Yap/Taz activities are increased in *Nf2* mutant brains and that overexpressing YAP in NPCs increases the abundance of GFAP$^+$ radial processes in the developing hippocampus (Lavado et al., 2013), a phenotype resembling that of *Nf2* mutant GW. Second, *SLIT2* is induced by YAP overexpression in several cell types and is considered a signature gene of enhanced YAP activity (Dupont et al., 2011; Mohseni et al., 2014; Zhao et al., 2008).

Development (2014) 141, 4182-4193 doi:10.1242/dev.111260

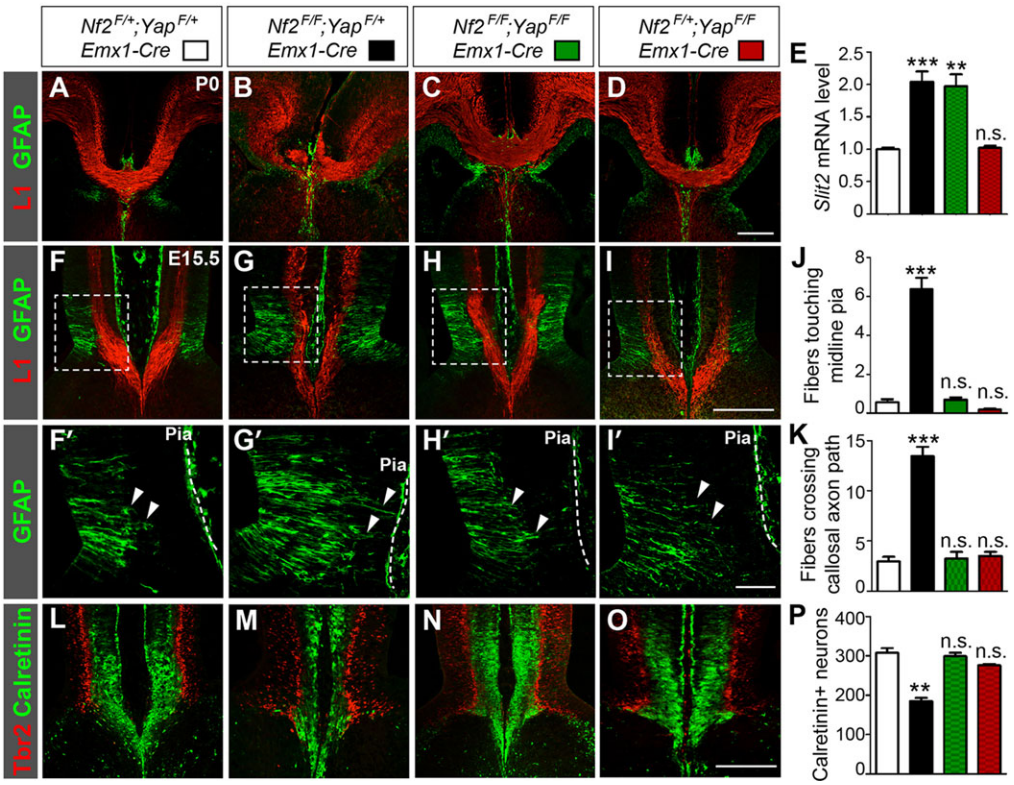

Fig. 6. *Yap* deletion restores the corpus callosum in *Nf2* mutants. (A-D) Sections of littermates show that deleting *Yap* in the $Nf2^{F/F}$;*Emx1-Cre* background restores the corpus callosum at P0 (C). (E) qRT-PCR analyses of E15.5 rostral medial-cortex tissues show that, compared with $Nf2^{F/+}$;$Yap^{F/+}$;*Emx1-Cre* controls, the *Slit2* mRNA level is upregulated in $Nf2^{F/F}$;$Yap^{F/F}$;*Emx1-Cre* animals, similar to that in $Nf2^{F/F}$;$Yap^{F/+}$;*Emx1-Cre* embryos. $Nf2^{F/+}$;$Yap^{F/+}$;*Emx1-Cre*, n=4; the rest, n=3. (F-K) *Yap* deletion rescues the GW defects of *Nf2* mutants. At E15.5, the number of GFAP$^+$ GW fibers (arrowheads) touching the midline pia and that crossing callosal axon path in $Nf2^{F/F}$;$Yap^{F/F}$;*Emx1-Cre* embryos are similar to those in littermate $Nf2^{F/+}$;$Yap^{F/+}$;*Emx1-Cre* controls. n=4. (L-P) The number of Calretinin$^+$ neurons is restored to control levels in the midline of $Nf2^{F/F}$;$Yap^{F/F}$;*Emx1-Cre* animals. n=3. Panels labeled with primes are magnified views of the boxed areas in corresponding panels. In panels E,J,K,P, statistical significance scores are evaluated against $Nf2^{F/+}$;$Yap^{F/+}$;*Emx1-Cre* embryos. **P<0.01; ***P<0.001; n.s., not significant. Scale bars: 200 µm, except 50 µm in I′.

If Yap overactivation is responsible for callosal agenesis in *Nf2* mutants, then deleting *Yap* should restore the corpus callosum. To test this, we generated *Nf2*;*Yap* double conditional mutants. Indeed, every double mutant examined between stages E17.5 and P0 developed the corpus callosum (n=10, Fig. 6C). Moreover, the formation of midline guideposts was completely restored in E15.5 *Nf2*;*Yap* double mutants. As in littermate $Nf2^{F/+}$;$Yap^{F/+}$;*Emx1-Cre* controls, few GW processes remained attached to the pia in *Nf2*;*Yap* double mutants (Fig. 6F-K, arrowheads). The number of Calretinin$^+$ neurons in *Nf2*;*Yap* double mutants was similar to that in $Nf2^{F/+}$;$Yap^{F/+}$;*Emx1-Cre* controls (Fig. 6L-P). However, qRT-PCR analysis of E15.5 rostral medial-cortex tissues showed that, in *Nf2*;*Yap* double mutants, the *Slit2* mRNA level remained upregulated compared with that of littermate $Nf2^{F/+}$;$Yap^{F/+}$;*Emx1-Cre* controls and was similar to that in $Nf2^{F/F}$;$Yap^{F/+}$;*Emx1-Cre* mutants (Fig. 6E). *Yap* deletion in the *Nf2* heterozygous background did not have obvious effects on guidepost development, *Slit2* level, or callosal formation (Fig. 6D,E,I-K,O,P). Taken together, these results strongly suggest that Yap overactivation, which disrupts guidepost development, contributes to callosal agenesis in *Nf2* mutants. Because Yap expression is restricted to NPCs (Milewski et al., 2004) (Fig. 7A), these results also suggest that Nf2 functions within NPCs to regulate callosal development. That *Slit2* remains upregulated in *Nf2*;*Yap* double mutants indicates that Taz overactivation might also contribute to *Slit2* upregulation.

Elevating YAP activity in midline NPCs causes callosal agenesis

To further confirm that aberrant Yap/Taz activation underlies callosal agenesis in *Nf2* mutants, we tested whether increasing their activity was sufficient to prevent callosal formation. Based on our finding that Nf2 is required to generate the proper midline environment, we predicted that elevating Yap/Taz activity selectively in midline NPCs would block callosal formation. To test this, we crossed mice carrying a doxycycline-inducible allele of human *YAP1*, *TetO-YAP1* (Camargo et al., 2007), with an *Axin2-rtTA* line that expresses the doxycycline-dependent transactivator rtTA from the *Axin2* promoter, which is active in the midline of the dorsal neural tube, including the dorsal telencephalic midline (Yu et al., 2007). Immunostaining confirmed that, in *TetO-YAP1*;*Axin2-rtTA* double-transgenic (dTG) embryos, the level of YAP was specifically increased in the midline ventricular zone but not in the rest of the brain (Fig. 7A,B, arrowheads). By measuring the fluorescence intensity of Yap/Taz immunostaining signals (supplementary material Fig. S8A,B), we estimated that the YAP protein level at the midline of E13.5 dTG embryos was 1.934±0.007 times greater than that in controls (n=3, P<0.0001). Quantitative western blot analysis of E16.5 medial-cortex tissues showed a 2.5±0.1 fold increase of YAP protein amount in dTG embryos (n=3, P<0.0001; supplementary material Fig. S8C).

The phenotypes of these dTG animals were strikingly similar to those of *Nf2* mutants – at E18.5, callosal axons in dTG brains approached the midline but few crossed it, instead forming Probst bundles (Fig. 7D, arrow). Some GW fibers penetrated the callosal axon path (Fig. 7D, arrowhead). Calretinin$^+$ guidepost neurons, instead of forming two bands dorsal and ventral to the corpus callosum as they did in controls (Fig. 7E), became disorganized, many invading the callosal axon path (Fig. 7F, arrowhead). Defects in midline development were evident at E16.5 and closely resembled those in *Nf2* mutants. The GW expanded dorsoventrally (Fig. 7G,H, white line) and numerous radial processes overextended to the pia (Fig. 7G′,H′, arrowhead). (The number of GFAP$^+$ processes touching the midline pia was 0.083±0.083 in controls and 6.67±0.08 in dTG; n=3, P<0.0001. The number of GFAP$^+$ processes crossing the callosal axon path was 1.7±0.3 in controls and 20.0±1.2 in dTG; n=3, P=0.0001.) Fewer Calretinin$^+$ guidepost neurons were present (Fig. 7I,J; 335±20 Calretinin$^+$ neurons in controls, 212±14 in dTG; n=3, P=0.007). Moreover, *Slit2* expression was markedly upregulated in dTG embryos, as shown by using *in situ* hybridization (Fig. 7K,L) and

Development (2014) 141, 4182-4193 doi:10.1242/dev.111260

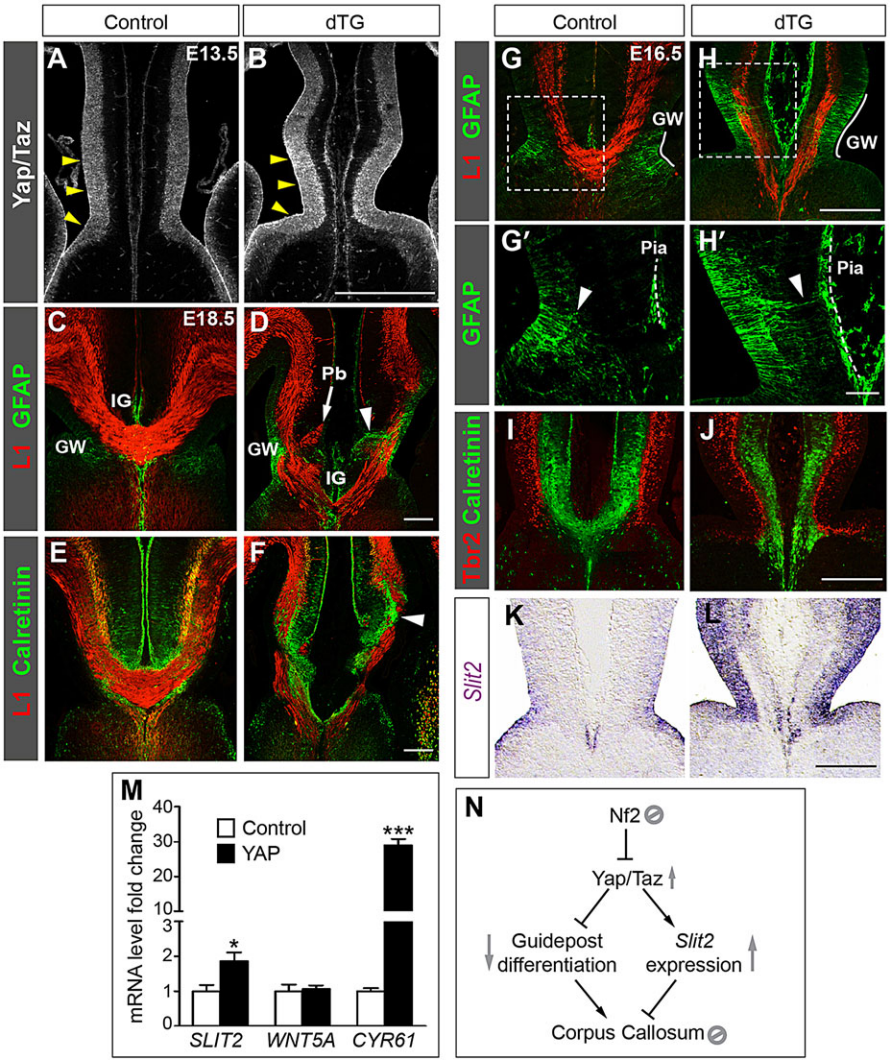

Fig. 7. Overexpressing YAP in midline NPCs causes callosal agenesis. (A,B) Immunostaining with an antibody recognizing Yap and Taz shows Yap/Taz expression in ventricular zone NPCs of control brains and increased expression specifically in the midline NPCs of *TetO-YAP1*;*Axin2-rtTA* double-transgenic (dTG) embryos (arrowheads). (C-F) dTG embryos at E18.5 exhibit callosal agenesis, with Probst bundles (Pb) accumulating at the midline (D, arrow), GW fibers protruding to the pia (D, arrowhead) and Calretinin^{+} guidepost neurons aggregating within the callosal axon path (F, arrowhead). *n*=4. (G-L) dTG embryos at E16.5 exhibit midline defects, including elongation of the GW (G,H, white line), extension of GW fibers (arrowhead) to the pia (dashed line) (G′,H′), fewer Calretinin^{+} neurons (I,J) and *Slit2* upregulation (using *in situ* hybridization) (K,L). Panels labeled with primes are magnified views of the boxed areas in corresponding panels. (M) qRT-PCR assays show that *YAP* overexpression in HEK293T cells increases the mRNA levels of *SLIT2* and *CYR61* but not *WNT5A*. *n*=3, **P*<0.05, ****P*<0.001. (N) Model of the signaling cascade delineated in this study. In midline neural progenitor cells, Nf2 suppresses Yap/Taz to promote guidepost differentiation and to prevent ectopic Slit2 expression, thus allowing the formation of the corpus callosum. See text for details. Scale bars: 200 µm, except 50 µm in H′.

qRT-PCR analyses of rostral medial-cortex tissues at E16.5 (1.5±0.1 fold increase in dTG, *n*=3, *P*=0.013), supporting the hypothesis that elevated Yap/Taz activities upregulate *Slit2* transcription. In summary, overexpressing YAP selectively in midline NPCs is sufficient to phenocopy the defects caused by *Nf2* deletion, further strengthening the hypothesis that Nf2 regulates callosal development by suppressing Yap/Taz activities in midline NPCs.

Next, we wanted to test whether Yap/Taz activate transcription of *Slit2*. The *Slit2* gene lies within a 2.5 Mb region (chr5:45860000-48370000) containing hundreds of evolutionarily conserved regions, which are potential enhancer elements (http://ecrbrowser.dcode.org/), making it very difficult to identify *cis*-regulatory elements and determine whether Yap/Taz directly act on them. We therefore took an indirect approach. We overexpressed YAP in HEK293T cells and then measured *SLIT2* mRNA levels using qRT-PCR analyses. Compared with vector-transfected cells, YAP-transfected cells expressed higher levels of *SLIT2*, as well as *CYR61*, a known YAP target gene (Fig. 7M). In comparison, YAP overexpression had no effect on the level of *WNT5A* (Fig. 7M), another callosal guidance cue that is expressed at the midline (Keeble et al., 2006). That YAP overexpression increases *SLIT2* transcript levels in HEK293T cells, a cell type unrelated to midline NPCs, strongly suggests that Yap/Taz regulate *Slit2* transcription and argues against the possibility that *Slit2* upregulation in *Nf2*-deletion or YAP-overexpression mutants was secondary to changes in the general properties of midline cells.

DISCUSSION

By dissecting the mechanism underlying the callosal agenesis caused by *Nf2* deletion, we discovered a signaling cascade operating within NPCs to control callosal axon pathfinding. We found that the Nf2 tumor suppressor inhibits Yap/Taz transcriptional coactivators in NPCs, which in turn regulate midline guidepost development and expression of the guidance cue Slit2, hence influencing the midline environment that callosal axons travel through and affecting their navigation. Nf2 loss leads to aberrant Yap/Taz activation, which impairs guidepost formation and induces *Slit2* expression, preventing callosal formation (Fig. 7N). We provide compelling genetic evidence for this signaling cascade by showing that *Yap* deletion and *Slit2* heterozygosity both restore the corpus callosum in *Nf2* mutants and that Yap gain-of-function selectively in midline NPCs prevents callosal formation. Nf2 and Yap/Taz are crucial components of the Hippo pathway, a conserved signaling pathway governing tissue growth and homeostasis (Yu and Guan, 2013), including mammalian brain growth (Lavado et al., 2013). In addition to offering new insights into the molecular regulation of midline development, our study demonstrates that perturbations in neural progenitor properties affect not only brain growth but also its

Development (2014) 141, 4182-4193 doi:10.1242/dev.111260

wiring, highlighting that growth and wiring are intricately coordinated during brain development.

Nf2 loss causes guidepost defects and *Slit2* upregulation. *Slit2* heterozygosity and *Yap* deletion both re-establish the corpus callosum in *Nf2* mutants. Interestingly, the former suppresses *Slit2* upregulation but does not fully rescue guidepost development at E15.5 (before midline crossing), whereas the latter rescues guidepost development but does not mitigate *Slit2* upregulation. These results suggest that both the guidepost defects and *Slit2* upregulation contribute to, but neither is sufficient to cause, callosal agenesis in *Nf2* mutants. Overexpressing YAP in midline NPCs, however, is sufficient to cause callosal agenesis and, importantly, both the guidepost defects and *Slit2* upregulation, closely mimicking the effects of Nf2 loss. These results strongly suggest that aberrant Yap/Taz activation is the cause of callosal agenesis in *Nf2* mutants, being responsible for both the guidepost defects and *Slit2* upregulation, and that elevated Taz activity accounts for *Slit2* upregulation in *Nf2*;*Yap* double mutants. This interpretation is consistent with our previous finding that the nuclear levels of both Yap and Taz proteins are increased in *Nf2* mutant brains (Lavado et al., 2013). Our results do not preclude that defects other than guidepost malformation and *Slit2* upregulation also contribute to callosal agenesis in *Nf2*-deletion and *YAP*-overexpression mutants. Furthermore, the apparent contradiction between the overexpression of Slit2 by using *in utero* electroporation resulting in abnormal axon tangles and the elevated levels of Slit2 in *Nf2*;*Yap* double mutants having little effect on callosal axon pathfinding is probably because *in utero* electroporation leads to higher levels of Slit2 than that found in *Nf2*;*Yap* double mutants.

Nf2 and Yap regulate the development of midline guideposts

Guidepost cells associated with the developing corpus callosum were first observed decades ago (Silver et al., 1982). Recent research using mouse mutants began to uncover the molecular mechanisms governing their development. A comparison of *Nf2* mutant phenotypes to those described previously reveals interesting similarities and differences that help us to better understand the role of Nf2 during guidepost development.

Nf2 mutants closely resemble *Gli3* hypomorphic and conditional knockout mutants, which have overextended GW processes, fewer Calretinin$^+$ guidepost neurons and increased *Slit2* levels (Amaniti et al., 2013; Magnani et al., 2014). However, it does not seem that *Nf2* mutant phenotypes are caused by altered Gli3 function. First, *Gli3* mutations lead to altered Fgf and Wnt signaling at the corticoseptal boundary and defective midline patterning (Amaniti et al., 2013; Magnani et al., 2014), whereas Fgf, Wnt signaling and midline patterning are unperturbed in *Nf2* mutants. Second, unlike in *Nf2* mutants, *Slit2* deletion in *Gli3* hypomorphic mutants does not restore the corpus callosum, consistent with *Gli3* hypomorphic mutants having an earlier and broader midline patterning defect. However, the levels of Gli3FL and Gli3R and the ratio of Gli3FL to Gli3R were increased in *Nf2* mutants, suggesting that Gli3 activator activities might be higher in *Nf2* mutants. This change in Gli3 activity would be in the same direction as that found in *Gli3* mutants because Gli3 is thought to mainly act in its repressor form in the developing cortex (Rallu et al., 2002). More molecular and genetic analyses are required to determine whether Nf2 and Gli3 functionally interact during callosal development.

We found that Nf2 promotes the transition of GW radial glia from those extending long radial processes to the pia to those having short processes. Whether this transition involves the former retracting their long processes or being replaced by radial glia born with short processes needs to be addressed through live-imaging experiments. In mice that lack Fgf receptor 1 in radial glia, GW radial glia fail to translocate from the ventricular zone to the IG. Consequently, in these mutants, GW processes remain attached to the pia at P0 and IG astrocytes are lacking (Smith et al., 2006). Fgf signaling-mediated radial glia translocation is unlikely to be involved in the GW phenotype of *Nf2* mutants because IG astrocytes are present and Fgf signaling is unperturbed in *Nf2* mutants.

Transcription factors Nfia and Nfib (Nfia,b) are also required for GW radial glia maturation (Shu et al., 2003a; Steele-Perkins et al., 2005). However, the GW defects of *Nfia*$^{-/-}$ and *Nfib*$^{-/-}$ mice are opposite to those of *Nf2* mutants – GFAP$^+$ processes are fewer and shorter in *Nfia*$^{-/-}$ mice than in wild-type animals and are mostly absent in *Nfib*$^{-/-}$ mice. We postulate that Nf2 and Nfia,b. act at different levels during GW radial glia development: Nf2, by inhibiting Yap, promotes the transition to later cellular states, whereas Nfia,b promote astroglial structural characteristics. Supporting this idea, it has been shown that Yap promotes stem cell and progenitor cell self-renewal in many systems (Barry and Camargo, 2013), whereas Nfi factors directly activate the expression of astroglial genes (Namihira et al., 2009).

We show that Nf2 promotes the differentiation of Calretinin$^+$ guidepost neurons. It is unclear which progenitor population gives rise to these neurons. The juxtaposition of these neurons with GW radial glia and the phenotypic correlation between the reduction in Calretinin$^+$ neuron production and delayed developmental transition of GW radial glia in *Nf2* mutants suggest that at least some Calretinin$^+$ guidepost neurons are derived from GW radial glia. Lineage-tracing experiments are required to determine whether this is the case. Intriguingly, these guidepost neurons share several features with Cajal–Retzius cells: both express Calretinin but are glutamatergic, whereas most if not all other cortical Calretinin$^+$ neurons are GABAergic; both exist transiently during development and both guide axonal navigation (Borrell et al., 2007; Del Rio et al., 1997). A source of Cajal–Retzius cells is the cortical hem, residing along the caudal telencephalic midline immediately posterior to the GW (Grove et al., 1998). It is plausible that these two anatomically and ontogenetically associated structures give rise to functionally similar progenies.

Deleting *Nf2* using *Emx1-Cre* does not affect anterior commissure formation, although *Emx1-Cre* is active in the NPCs that give rise to neurons projecting through the anterior commissure (Falk et al., 2005; Gorski et al., 2002). Interestingly, formation of the anterior commissure is abolished when *Nf2* is removed throughout the nervous system by *Nestin-Cre* (supplementary material Fig. S1D). These contrasting results suggest that Nf2 is likely to be required for the development of the ventral midline environment where the anterior commissure forms. GFAP$^+$ glia are found surrounding the developing anterior commissure (Lent et al., 2005; Pires-Neto et al., 1998; Silver et al., 1993), although their origin and function have not been established. Future studies are required to determine whether Nf2-Yap signaling regulates the development of these putative anterior commissure guidepost cells and those involved in the formation of other axon tracts (Chedotal and Richards, 2010).

Nf2 and Yap/Taz regulate *Slit2* expression

Remarkable progress has been made in identifying axon guidance molecules and elucidating their functions. Although it is self-evident that these molecules must be expressed at the correct place and time for proper wiring, how their expression is regulated is poorly understood. Here, we show that Nf2 suppresses Yap/Taz to prevent aberrant *Slit2* expression. Our finding is clearly just a small part of

Development (2014) 141, 4182-4193 doi:10.1242/dev.111260

Slit2 transcriptional control. The *Slit2* gene exhibits complex expression patterns during brain development (Borrell et al., 2012; Unni et al., 2012). The large and conserved non-coding region of the gene suggests multifaceted transcriptional regulation. A recent study has elegantly demonstrated that a small difference in *Slit2* expression patterns in mammals and birds leads to different positioning of guidepost neurons and ultimately divergent trajectories of thalamic axons in these two species (Bielle et al., 2011). Future studies on the transcriptional regulation of guidance molecules will provide deeper understanding of how the nervous system is wired during organism development and species evolution.

MATERIALS AND METHODS

Animals

Animal experiments were performed in accordance with the guidelines of the Institutional Animal Care and Use Committee of St. Jude Children's Research Hospital (SJCRH). *Emx1*$^{IRES\text{-}Cre}$ (stock: 005628), *Nestin-Cre* (003771), *Rosa-CAG-LSL-tdTomato* (007909), *Rosa-CAG-LSL-ZsGreen* (007906) and *Axin2-rtTA* (016997) lines were from the Jackson Laboratory. *Nf2*$^{F/F}$, *Yap*$^{F/F}$ (Xin et al., 2011) and *TetO-YAP1* lines were provided by Marco Giovannini (University of California Los Angeles, CA, USA), Eric Olson (UT Southwestern Medical Center, Dallas, TX, USA) and Fernando Camargo (Boston Children's Hospital, MA, USA), respectively. *Satb2-Cre* (032908-UCD) and *Slit2*$^{+/-}$ (Plump et al., 2002) lines were obtained from the Mutant Mouse Regional Resource Center (MMRRC) at University of California Davis (Davis, CA, USA) and University of Missouri (Columbia, MO, USA), respectively. All experimental animals were in mixed background. Littermates were used for comparison studies. Doxycycline was administered in drinking water (E9.5-14.5, 100 mg/l; E14.5-18.5, 200 mg/l). For BrdU labeling, timed pregnant mice were intraperitoneally injected with BrdU at 100 mg/kg.

Histology, immunostaining and *in situ* hybridization

Luxol Blue and Cresyl Violet staining was performed on 8 µm thick paraffin sections using the Kluver–Barrera method (EMS no. 26681). Immunostaining was performed on 10 to 14 µm thick cryosections. Details are provided in supplementary Materials and Methods. Primary antibodies are listed in supplementary material Table S1. Fluorescent secondary antibodies were from Jackson ImmunoResearch. *In situ* hybridization was performed as described previously (Schaeren-Wiemers and Gerfin-Moser, 1993) using the following probes: *Slit2* and *Robo1* (Brose et al., 1999), *Netrin1* (Serafini et al., 1996), *Sema3c* (Bagnard et al., 1998), *Draxin* (Islam et al., 2009), *Fgf8* (Crossley and Martin, 1995), *Sprouty1* (Minowada et al., 1999), *Wnt8b* (Liu et al., 2010) and *Axin2* (Andoniadou et al., 2007) (supplementary material Table S2). Low-magnification images were acquired with a Zeiss AxioImager M2 microscope. The remaining images were acquired with Zeiss LSM510 or LSM780 confocal microscopes. For measuring the fluorescence intensities of Yap/Taz immunostaining signals, single-plane confocal images with signals below saturation levels were captured using the same settings for control and dTG samples. Quantification was performed on sections of comparable levels. The values shown are mean±s.e.m. per section of the indicated number of animals, and the value of each animal is the average of six sections. Statistical significance was evaluated by using two-tailed unpaired *t*-tests.

Transplantation and slice culture

Transplantation and slice culture procedures were performed as described previously (Niquille et al., 2009). Briefly, brains at E16.5 were dissected in cold Hank's balanced salt solution (HBSS) and embedded in 3% low-melting agarose (Invitrogen). Using a Vibratome, 300 µm thick coronal sections were obtained. After transplantation, slices were cultured for 72 h on Nucleopore Track-Etch Membranes (1-µm pore size, Whatman) in a 3:1 mixture of basal medium Eagle (BME) and HBSS supplemented with glucose, glutamine, 5% horse serum and penicillin-streptomycin (Invitrogen). Transplants showing axon growth toward the midline were included in the analysis.

In utero electroporation

In utero electroporation was performed as described previously (Saito, 2006). Briefly, the plasmid solution was microinjected into forebrain ventricles of embryos at E13.5 *in utero*, and square-wave electric pulses (40 V, five pulses with durations of 50 ms/pulse and at 1-second intervals) were delivered with Tweezertrodes connected to an ECM 830 electroporator (Harvard Apparatus). Embryos were returned to the dam and harvested 4 days later.

Western blot, qRT-PCR, cell culture and transfection

For western blot analyses, tissues were homogenized in 20 mM HEPES (pH 7.4), 150 mM NaCl, 5% glycerol, 2% SDS supplemented with Halt protease and phosphatase inhibitors (Thermo Scientific). Quantitative western blot was performed using IRDye 600LT- and 800CW-conjugated secondary antibodies, which were then detected with the ODYSSEY infrared imaging system (LI-COR). Primary antibodies are listed in supplementary material Table S1. HEK293T cells were cultured in Dulbecco's modified Eagle's medium (DMEM) containing 10% fetal bovine serum (Invitrogen), transfected with Lipofectamine 2000 (Invitrogen) and then harvested 48 h later. RNA was isolated using Trizol (Invitrogen). cDNA was prepared with SuperScript III reverse transcriptase (Life Technologies). qRT-PCR reactions were performed with Fast SYBR Master Mix (Life Technologies) using the primers listed in supplementary material Table S3. Values are mean±s.e.m. Statistical significance was evaluated by using two-tailed unpaired *t*-tests.

Acknowledgements

We thank Marco Giovannini, Eric Olson and Fernando Camargo for sharing mouse lines; Marc Tessier-Lavigne, Jean Hébert, Avraham Yaron, Richard Lang, Gail Martin and Kun-Liang Guan for plasmids; Guillermo Oliver for an antibody against Six3; MMRRC, GENSAT and INSERM (France) for mouse lines; Addgene for plasmids; SJCRH Imaging Center for assistance with image acquisition; Jim Morgan, David Solecki, Young-Goo Han and Ge Bai for suggestions on the manuscript and Cherise Guess for editorial assistance.

Competing interests

The authors declare no competing financial interests.

Author contributions

X.C. conceived the project. X.C., A.L. and M.W. designed the experiments and analyzed the results. A.L. performed most of the experiments. M.W. performed initial studies. J.P. performed Luxol Blue staining, western blot, qRT-PCR and HEK293T cell experiments. X.C. collected tissues for western blot and qRT-PCR assays and performed *in utero* electroporation. X.C. wrote and A.L. edited the manuscript.

Funding

This work was supported by American Lebanese Syrian Associated Charities; Basil O'Connor Award [5-FY10-488] from March of Dimes; the Whitehall Foundation [2012-05-106]; and the National Institutes of Health [R01NS086938]. The Imaging Center is supported by SJCRH and the National Cancer Institute [grant P30 CA021765-34]. Deposited in PMC for release after 12 months.

Supplementary material

Supplementary material available online at
http://dev.biologists.org/lookup/suppl/doi:10.1242/dev.111260/-/DC1

References

Alcamo, E. A., Chirivella, L., Dautzenberg, M., Dobreva, G., Fariñas, I., Grosschedl, R. and McConnell, S. K. (2008). Satb2 regulates callosal projection neuron identity in the developing cerebral cortex. *Neuron* **57**, 364-377.

Amaniti, E.-M., Hasenpusch-Theil, K., Li, Z., Magnani, D., Kessaris, N., Mason, J. O. and Theil, T. (2013). Gli3 is required in Emx1(+) progenitors for the development of the corpus callosum. *Dev. Biol.* **376**, 113-124.

Andoniadou, C. L., Signore, M., Sajedi, E., Gaston-Massuet, C., Kelberman, D., Burns, A. J., Itasaki, N., Dattani, M. and Martinez-Barbera, J. P. (2007). Lack of the murine homeobox gene Hesx1 leads to a posterior transformation of the anterior forebrain. *Development* **134**, 1499-1508.

Andrews, W., Liapi, A., Plachez, C., Camurri, L., Zhang, J., Mori, S., Murakami, F., Parnavelas, J. G., Sundaresan, V. and Richards, L. J. (2006). Robo1 regulates the development of major axon tracts and interneuron migration in the forebrain. *Development* **133**, 2243-2252.

Bagnard, D., Lohrum, M., Uziel, D., Puschel, A. W. and Bolz, J. (1998). Semaphorins act as attractive and repulsive guidance signals during the development of cortical projections. *Development* **125**, 5043-5053.
Bagri, A., Marín, O., Plump, A. S., Mak, J., Pleasure, S. J., Rubenstein, J. L. R. and Tessier-Lavigne, M. (2002). Slit proteins prevent midline crossing and determine the dorsoventral position of major axonal pathways in the mammalian forebrain. *Neuron* **33**, 233-248.
Barry, E. R. and Camargo, F. D. (2013). The Hippo superhighway: signaling crossroads converging on the Hippo/Yap pathway in stem cells and development. *Curr. Opin. Cell Biol.* **9**, 6.
Benadiba, C., Magnani, D., Niquille, M., Morlé, L., Valloton, D., Nawabi, H., Ait-Lounis, A., Otsmane, B., Reith, W., Theil, T. et al. (2012). The ciliogenic transcription factor RFX3 regulates early midline distribution of guidepost neurons required for corpus callosum development. *PLoS Genet.* **8**, e1002606.
Bielle, F., Marcos-Mondejar, P., Keita, M., Mailhes, C., Verney, C., Nguyen Ba-Charvet, K., Tessier-Lavigne, M., Lopez-Bendito, G. and Garel, S. (2011). Slit2 activity in the migration of guidepost neurons shapes thalamic projections during development and evolution. *Neuron* **69**, 1085-1098.
Borrell, V., Pujadas, L., Simó, S., Durà, D., Solé, M., Cooper, J. A., Del Río, J. A. and Soriano, E. (2007). Reelin and mDab1 regulate the development of hippocampal connections. *Mol. Cell. Neurosci.* **36**, 158-173.
Borrell, V., Cárdenas, A., Ciceri, G., Galcerán, J., Flames, N., Pla, R., Nóbrega-Pereira, S., García-Frigola, C., Peregrín, S., Zhao, Z. et al. (2012). Slit/Robo signaling modulates the proliferation of central nervous system progenitors. *Neuron* **76**, 338-352.
Britanova, O., de Juan Romero, C., Cheung, A., Kwan, K. Y., Schwark, M., Gyorgy, A., Vogel, T., Akopov, S., Mitkovski, M., Agoston, D. et al. (2008). Satb2 is a postmitotic determinant for upper-layer neuron specification in the neocortex. *Neuron* **57**, 378-392.
Brose, K., Bland, K. S., Wang, K. H., Arnott, D., Henzel, W., Goodman, C. S., Tessier-Lavigne, M. and Kidd, T. (1999). Slit proteins bind Robo receptors and have an evolutionarily conserved role in repulsive axon guidance. *Cell* **96**, 795-806.
Camargo, F. D., Gokhale, S., Johnnidis, J. B., Fu, D., Bell, G. W., Jaenisch, R. and Brummelkamp, T. R. (2007). YAP1 increases organ size and expands undifferentiated progenitor cells. *Curr. Biol.* **17**, 2054-2060.
Chedotal, A. and Richards, L. J. (2010). Wiring the brain: the biology of neuronal guidance. *Cold Spring Harb. Perspect. Biol.* **2**, a001917.
Chinn, G. A., Hirokawa, K. E., Chuang, T. M., Urbina, C., Patel, F., Fong, J., Funatsu, N. and Monuki, E. S. (2014). Agenesis of the corpus callosum due to defective glial wedge formation in Lhx2 mutant mice. *Cereb. Cortex* (in press).
Clegg, J. M., Conway, C. D., Howe, K. M., Price, D. J., Mason, J. O., Turnbull, J. E., Basson, M. A. and Pratt, T. (2014). Heparan sulfotransferases Hs6st1 and Hs2st keep Erk in check for mouse corpus callosum development. *J. Neurosci.* **34**, 2389-2401.
Crossley, P. H. and Martin, G. R. (1995). The mouse Fgf8 gene encodes a family of polypeptides and is expressed in regions that direct outgrowth and patterning in the developing embryo. *Development* **121**, 439-451.
Del Río, J. A., Heimrich, B., Borrell, V., Förster, E., Drakew, A., Alcántara, S., Nakajima, K., Miyata, T., Ogawa, M., Mikoshiba, K. et al. (1997). A role for Cajal-Retzius cells and reelin in the development of hippocampal connections. *Nature* **385**, 70-74.
Donahoo, A.-L. S. and Richards, L. J. (2009). Understanding the mechanisms of callosal development through the use of transgenic mouse models. *Semin. Pediatr. Neurol.* **16**, 127-142.
Dupont, S., Morsut, L., Aragona, M., Enzo, E., Giulitti, S., Cordenonsi, M., Zanconato, F., Le Digabel, J., Forcato, M., Bicciato, S. et al. (2011). Role of YAP/TAZ in mechanotransduction. *Nature* **474**, 179-183.
Falk, J., Bechara, A., Fiore, R., Nawabi, H., Zhou, H., Hoyo-Becerra, C., Bozon, M., Rougon, G., Grumet, M., Püschel, A. W. et al. (2005). Dual functional activity of semaphorin 3B is required for positioning the anterior commissure. *Neuron* **48**, 63-75.
Fame, R. M., MacDonald, J. L. and Macklis, J. D. (2011). Development, specification, and diversity of callosal projection neurons. *Trends Neurosci.* **34**, 41-50.
Fazeli, A., Dickinson, S. L., Hermiston, M. L., Tighe, R. V., Steen, R. G., Small, C. G., Stoeckli, E. T., Keino-Masu, K., Masu, M., Rayburn, H. et al. (1997). Phenotype of mice lacking functional Deleted in colorectal cancer (Dcc) gene. *Nature* **386**, 796-804.
Giovannini, M., Robanus-Maandag, E., van der Valk, M., Niwa-Kawakita, M., Abramowski, V., Goutebroze, L., Woodruff, J. M., Berns, A. and Thomas, G. (2000). Conditional biallelic Nf2 mutation in the mouse promotes manifestations of human neurofibromatosis type 2. *Genes Dev.* **14**, 1617-1630.
Gorski, J. A., Talley, T., Qiu, M., Puelles, L., Rubenstein, J. L. and Jones, K. R. (2002). Cortical excitatory neurons and glia, but not GABAergic neurons, are produced in the Emx1-expressing lineage. *J. Neurosci.* **22**, 6309-6314.
Grove, E. A., Tole, S., Limon, J., Yip, L. and Ragsdale, C. W. (1998). The hem of the embryonic cerebral cortex is defined by the expression of multiple Wnt genes and is compromised in Gli3-deficient mice. *Development* **125**, 2315-2325.
Houshmandi, S. S., Emnett, R. J., Giovannini, M. and Gutmann, D. H. (2009). The neurofibromatosis 2 protein, merlin, regulates glial cell growth in an ErbB2- and Src-dependent manner. *Mol. Cell. Biol.* **29**, 1472-1486.
Islam, S. M., Shinmyo, Y., Okafuji, T., Su, Y., Naser, I. B., Ahmed, G., Zhang, S., Chen, S., Ohta, K., Kiyonari, H. et al. (2009). Draxin, a repulsive guidance protein for spinal cord and forebrain commissures. *Science* **323**, 388-393.
Keeble, T. R., Halford, M. M., Seaman, C., Kee, N., Macheda, M., Anderson, R. B., Stacker, S. A. and Cooper, H. M. (2006). The Wnt receptor Ryk is required for Wnt5a-mediated axon guidance on the contralateral side of the corpus callosum. *J. Neurosci.* **26**, 5840-5848.
Koester, S. E. and O'Leary, D. D. (1994). Axons of early generated neurons in cingulate cortex pioneer the corpus callosum. *J. Neurosci.* **14**, 6608-6620.
Kriegstein, A. and Alvarez-Buylla, A. (2009). The glial nature of embryonic and adult neural stem cells. *Annu. Rev. Neurosci.* **32**, 149-184.
Lavado, A., He, Y., Pare, J., Neale, G., Olson, E. N., Giovannini, M. and Cao, X. (2013). Tumor suppressor Nf2 limits expansion of the neural progenitor pool by inhibiting Yap/Taz transcriptional coactivators. *Development* **140**, 3323-3334.
Lent, R., Uziel, D., Baudrimont, M. and Fallet, C. (2005). Cellular and molecular tunnels surrounding the forebrain commissures of human fetuses. *J. Comp. Neurol.* **483**, 375-382.
Li, W., Cooper, J., Karajannis, M. A. and Giancotti, F. G. (2012). Merlin: a tumour suppressor with functions at the cell cortex and in the nucleus. *EMBO Rep.* **13**, 204-215.
Liu, W., Lagutin, O., Swindell, E., Jamrich, M. and Oliver, G. (2010). Neuroretina specification in mouse embryos requires Six3-mediated suppression of Wnt8b in the anterior neural plate. *J. Clin. Invest.* **120**, 3568-3577.
Madisen, L., Zwingman, T. A., Sunkin, S. M., Oh, S. W., Zariwala, H. A., Gu, H., Ng, L. L., Palmiter, R. D., Hawrylycz, M. J., Jones, A. R. et al. (2010). A robust and high-throughput Cre reporting and characterization system for the whole mouse brain. *Nat. Neurosci.* **13**, 133-140.
Magnani, D., Hasenpusch-Theil, K., Benadiba, C., Yu, T., Basson, M. A., Price, D. J., Lebrand, C. and Theil, T. (2014). Gli3 controls corpus callosum formation by positioning midline guideposts during telencephalic patterning. *Cereb. Cortex* **24**, 186-198.
McLaughlin, M. E., Kruger, G. M., Slocum, K. L., Crowley, D., Michaud, N. A., Huang, J., Magendantz, M. and Jacks, T. (2007). The Nf2 tumor suppressor regulates cell-cell adhesion during tissue fusion. *Proc. Natl. Acad. Sci. USA* **104**, 3261-3266.
Milewski, R. C., Chi, N. C., Li, J., Brown, C., Lu, M. M. and Epstein, J. A. (2004). Identification of minimal enhancer elements sufficient for Pax3 expression in neural crest and implication of Tead2 as a regulator of Pax3. *Development* **131**, 829-837.
Minowada, G., Jarvis, L. A., Chi, C. L., Neubuser, A., Sun, X., Hacohen, N., Krasnow, M. A. and Martin, G. R. (1999). Vertebrate Sprouty genes are induced by FGF signaling and can cause chondrodysplasia when overexpressed. *Development* **126**, 4465-4475.
Mohseni, M., Sun, J., Lau, A., Curtis, S., Goldsmith, J., Fox, V. L., Wei, C., Frazier, M., Samson, O., Wong, K.-K. et al. (2014). A genetic screen identifies an LKB1-MARK signalling axis controlling the Hippo-YAP pathway. *Nat. Cell Biol.* **16**, 108-117.
Moldrich, R. X., Gobius, I., Pollak, T., Zhang, J., Ren, T., Brown, L., Mori, S., De Juan Romero, C., Britanova, O., Tarabykin, V. et al. (2010). Molecular regulation of the developing commissural plate. *J. Comp. Neurol.* **518**, 3645-3661.
Namihira, M., Kohyama, J., Semi, K., Sanosaka, T., Deneen, B., Taga, T. and Nakashima, K. (2009). Committed neuronal precursors confer astrocytic potential on residual neural precursor cells. *Dev. Cell* **16**, 245-255.
Niquille, M., Garel, S., Mann, F., Hornung, J.-P., Otsmane, B., Chevalley, S., Parras, C., Guillemot, F., Gaspar, P., Yanagawa, Y. et al. (2009). Transient neuronal populations are required to guide callosal axons: a role for semaphorin 3C. *PLoS Biol.* **7**, e1000230.
Nishikimi, M., Oishi, K. and Nakajima, K. (2013). Axon guidance mechanisms for establishment of callosal connections. *Neural Plast.* **2013**, 149060.
Paul, L. K., Brown, W. S., Adolphs, R., Tyszka, J. M., Richards, L. J., Mukherjee, P. and Sherr, E. H. (2007). Agenesis of the corpus callosum: genetic, developmental and functional aspects of connectivity. *Nat. Rev. Neurosci.* **8**, 287-299.
Piper, M., Moldrich, R. X., Lindwall, C., Little, E., Barry, G., Mason, S., Sunn, N., Kurniawan, N. D., Gronostajski, R. M. and Richards, L. J. (2009a). Multiple non-cell-autonomous defects underlie neocortical callosal dysgenesis in Nfib-deficient mice. *Neural Dev.* **4**, 43.
Piper, M., Plachez, C., Zalucki, O., Fothergill, T., Goudreau, G., Erzurumlu, R., Gu, C. and Richards, L. J. (2009b). Neuropilin 1-Sema signaling regulates crossing of cingulate pioneering axons during development of the corpus callosum. *Cereb. Cortex* **19** Suppl. 1, i11-i21.
Pires-Neto, M. A., Braga-De-Souza, S. and Lent, R. (1998). Molecular tunnels and boundaries for growing axons in the anterior commissure of hamster embryos. *J. Comp. Neurol.* **399**, 176-188.
Plump, A. S., Erskine, L., Sabatier, C., Brose, K., Epstein, C. J., Goodman, C. S., Mason, C. A. and Tessier-Lavigne, M. (2002). Slit1 and Slit2 cooperate to

prevent premature midline crossing of retinal axons in the mouse visual system. *Neuron* **33**, 219-232.
Rallu, M., Machold, R., Gaiano, N., Corbin, J. G., McMahon, A. P. and Fishell, G. (2002). Dorsoventral patterning is established in the telencephalon of mutants lacking both Gli3 and Hedgehog signaling. *Development* **129**, 4963-4974.
Rash, B. G. and Richards, L. J. (2001). A role for cingulate pioneering axons in the development of the corpus callosum. *J. Comp. Neurol.* **434**, 147-157.
Saito, T. (2006). In vivo electroporation in the embryonic mouse central nervous system. *Nat. Protoc.* **1**, 1552-1558.
Schaeren-Wiemers, N. and Gerfin-Moser, A. (1993). A single protocol to detect transcripts of various types and expression levels in neural tissue and cultured cells: in situ hybridization using digoxigenin-labelled cRNA probes. *Histochemistry* **100**, 431-440.
Schulz, A., Baader, S. L., Niwa-Kawakita, M., Jung, M. J., Bauer, R., Garcia, C., Zoch, A., Schacke, S., Hagel, C., Mautner, V.-F. et al. (2013). Merlin isoform 2 in neurofibromatosis type 2-associated polyneuropathy. *Nat. Neurosci.* **16**, 426-433.
Serafini, T., Colamarino, S. A., Leonardo, E. D., Wang, H., Beddington, R., Skarnes, W. C. and Tessier-Lavigne, M. (1996). Netrin-1 is required for commissural axon guidance in the developing vertebrate nervous system. *Cell* **87**, 1001-1014.
Shu, T. and Richards, L. J. (2001). Cortical axon guidance by the glial wedge during the development of the corpus callosum. *J. Neurosci.* **21**, 2749-2758.
Shu, T., Butz, K. G., Plachez, C., Gronostajski, R. M. and Richards, L. J. (2003a). Abnormal development of forebrain midline glia and commissural projections in Nfia knock-out mice. *J. Neurosci.* **23**, 203-212.
Shu, T., Puche, A. C. and Richards, L. J. (2003b). Development of midline glial populations at the corticoseptal boundary. *J. Neurobiol.* **57**, 81-94.
Silver, J., Lorenz, S. E., Wahlsten, D. and Coughlin, J. (1982). Axonal guidance during development of the great cerebral commissures: descriptive and experimental studies, in vivo, on the role of preformed glial pathways. *J. Comp. Neurol.* **210**, 10-29.
Silver, J., Edwards, M. A. and Levitt, P. (1993). Immunocytochemical demonstration of early appearing astroglial structures that form boundaries and pathways along axon tracts in the fetal brain. *J. Comp. Neurol.* **328**, 415-436.
Smith, K. M., Ohkubo, Y., Maragnoli, M. E., Rasin, M.-R., Schwartz, M. L., Sestan, N. and Vaccarino, F. M. (2006). Midline radial glia translocation and corpus callosum formation require FGF signaling. *Nat. Neurosci.* **9**, 787-797.
Steele-Perkins, G., Plachez, C., Butz, K. G., Yang, G., Bachurski, C. J., Kinsman, S. L., Litwack, E. D., Richards, L. J. and Gronostajski, R. M. (2005). The transcription factor gene Nfib is essential for both lung maturation and brain development. *Mol. Cell. Biol.* **25**, 685-698.
Tronche, F., Kellendonk, C., Kretz, O., Gass, P., Anlag, K., Orban, P. C., Bock, R., Klein, R. and Schutz, G. (1999). Disruption of the glucocorticoid receptor gene in the nervous system results in reduced anxiety. *Nat. Genet.* **23**, 99-103.
Unni, D. K., Piper, M., Moldrich, R. X., Gobius, I., Liu, S., Fothergill, T., Donahoo, A.-L. S., Baisden, J. M., Cooper, H. M. and Richards, L. J. (2012). Multiple Slits regulate the development of midline glial populations and the corpus callosum. *Dev. Biol.* **365**, 36-49.
Xin, M., Kim, Y., Sutherland, L. B., Qi, X., McAnally, J., Schwartz, R. J., Richardson, J. A., Bassel-Duby, R. and Olson, E. N. (2011). Regulation of insulin-like growth factor signaling by Yap governs cardiomyocyte proliferation and embryonic heart size. *Sci. Signal.* **4**, ra70.
Yu, F.-X. and Guan, K.-L. (2013). The Hippo pathway: regulators and regulations. *Genes Dev.* **27**, 355-371.
Yu, H.-M. I., Liu, B., Costantini, F. and Hsu, W. (2007). Impaired neural development caused by inducible expression of Axin in transgenic mice. *Mech. Dev.* **124**, 146-156.
Zhao, B., Ye, X., Yu, J., Li, L., Li, W., Li, S., Yu, J., Lin, J. D., Wang, C.-Y., Chinnaiyan, A. M. et al. (2008). TEAD mediates YAP-dependent gene induction and growth control. *Genes Dev.* **22**, 1962-1971.

Supplementary Materials and Methods

Immunostaining

Mouse brains were dissected in PBS and fixed overnight in 4% paraformaldahyde in PBS at 4°C. Brains were then cryoprotected using 30% sucrose in PBS overnight at 4°C and embedded in OCT for cryosectioning. Frozen sections were washed with 0.2% Triton X-100 in TBS (TBST) and incubated in the blocking solution (3% normal donkey serum in TBST) for 1 hour at room temperature. Sections were incubated with primary antibodies (Table S1) diluted in the blocking solution overnight at 4°C, washed with TBST, and incubated with DyLight- or Alexa Fluor-conjugated secondary antibodies (Jackson ImmunoResearch) diluted at 1:1000 in the blocking solution for 2 hours at room temperature. Sections were counterstained with DAPI, washed in TBST, and mounted in ProLong Gold antifade reagent (Invitrogen). For BrdU detection, sections were first treated with 1N HCl at 45°C for 30 minutes, washed with TBST, and processed as above using an anti-BrdU antibody. For costaining using an anti-BrdU antibody and other primary antibodies, sections were first stained with the other primary antibodies, cross-linked in 4% paraformaldahyde in PBS for 20 minutes at room temperature, then stained with the anti-BrdU antibody.

Fig S1 Lavado et al

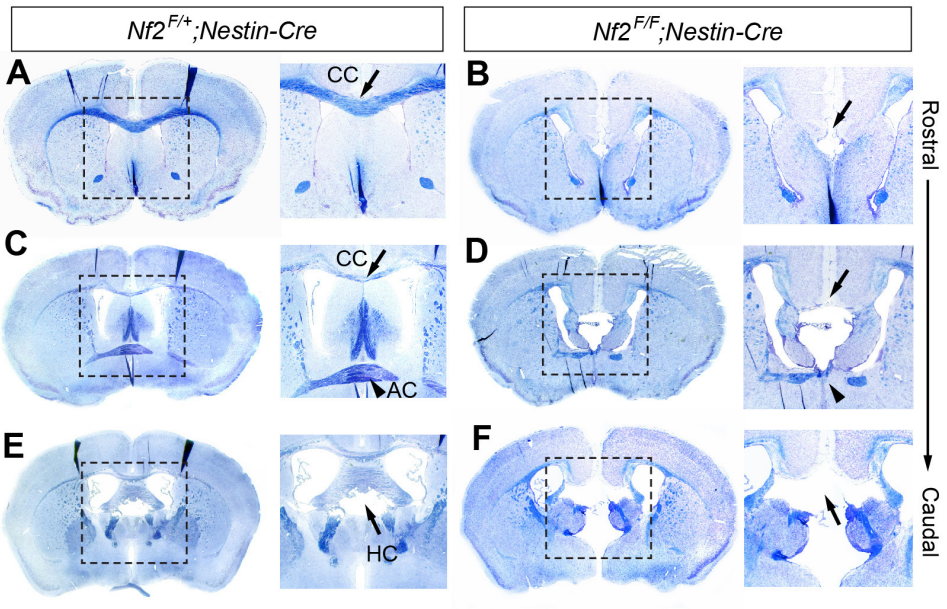

Fig. S1. Deleting *Nf2* with *Nestin-Cre* leads to agenesis of forebrain commissures. Luxol blue staining of myelinated axons (blue) and cresyl violet staining of neuronal cell bodies (purple) showing agenesis of the corpus callosum (CC) (A–D, arrow), anterior commissure (AC) (C,D, arrowhead), and hippocampal commissure (HC) (E,F, arrow) in 2-month–old *Nf2$^{F/F}$;Nestin-Cre* mice. *n*=3. A magnified view of the boxed region is shown in the image to the right.

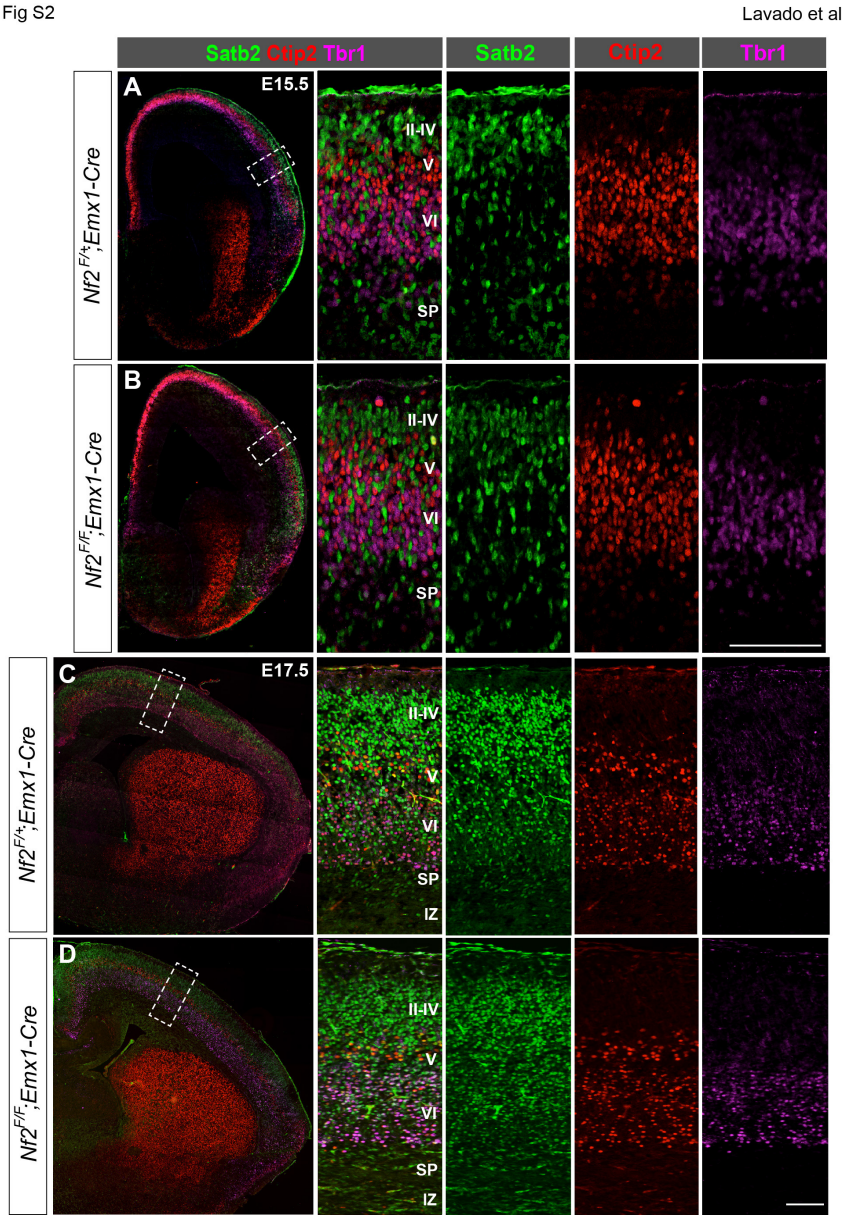

Fig. S2. Specification and production of callosal neurons are unaffected in *Nf2* mutants. Co-immunostaining showing proper expression of the callosal neuron–specific marker Satb2 in *Nf2*$^{F/F}$*;Emx1-Cre* neocortex and its proper laminar organization at E15.5 and E17.5. Images in the left column show low-magnified views. Regions in dashed boxes are enlarged in images to the right. SP: subplate; IZ: intermediate zone. Scale bars: 50 μm.

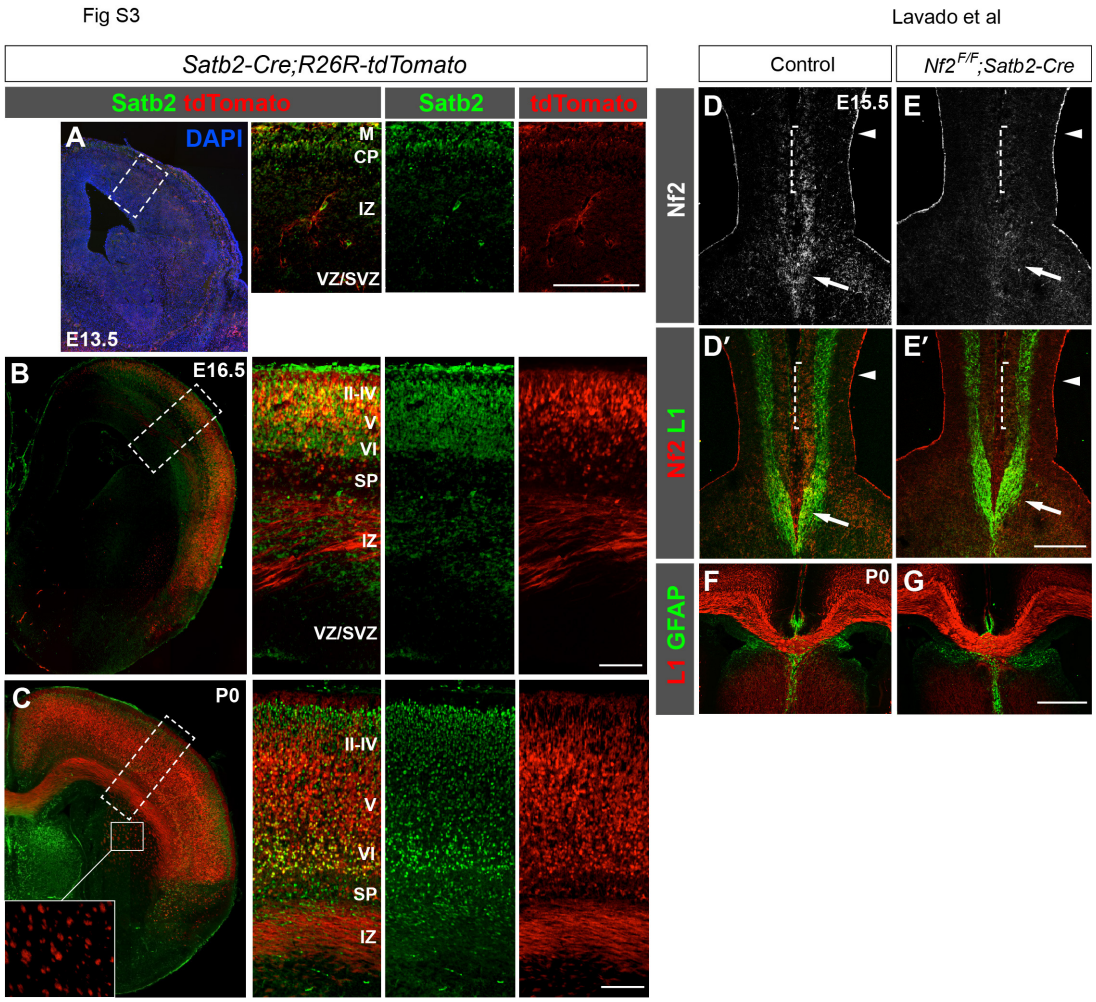

Fig. S3. Deleting *Nf2* in callosal neurons by using *Satb2-Cre* does not affect corpus callosum formation. (**A–C**) Co-immunostaining of Satb2 and tdTomato shows tdTomato expression in Satb2^{+} callosal neurons but not in ventricular zone and subventricular zone (VZ/SVZ) progenitor cells. TdTomato expression depends on Cre-mediated excision of the *LSL* (*loxP-stop-loxP*)-cassette in the *R26R-tdTomato* allele. As a consequence, tdTomato expression lags slightly behind Satb2 expression, which is likely why most Satb2^{+} cells at E13.5 are tdTomato-negative (A), as are the uppermost layer of Satb2^{+} cells at P0 (C). Inset in C shows a magnified view of the internal capsule, which also contains tdTomato-labeled axons. CP: cortical plate; IZ: intermediate zone; M: meninges; SP: subplate. (**D–E′**) In E15.5 *Nf2$^{F/F}$;Satb2-Cre* brains, Nf2 immunoreactivity in the cortical plate (dashed bracket) and callosal axons (arrow) is eliminated but that in the ventricular surface (arrowhead) is unperturbed. (**F**,**G**) The corpus callosum forms normally in P0 *Nf2$^{F/F}$;Satb2-Cre* brains. Scale bars: 50 μm in A,B,C; 200 μm in E′; 500 μm in G.

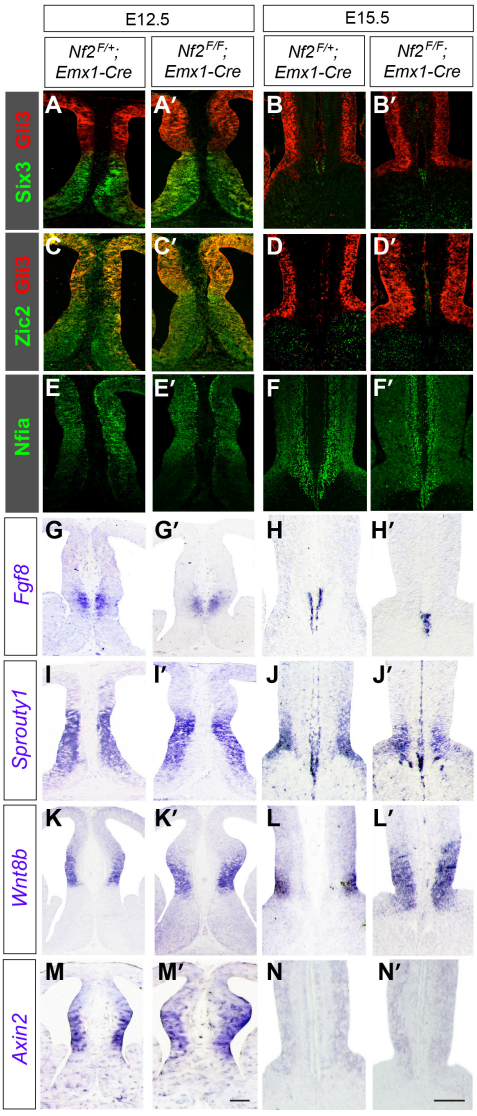

Fig. S4. Patterning of the corticoseptal boundary is grossly normal in *Nf2* mutants. Immunostaining and *in situ* hybridization show proper expression of Six3, Zic2, Nfia (transcription factors that delineate subdomains of the commissural plate), Gli3, *Fgf8* (molecules required for corticoseptal boundary patterning), *Sprouty1*, *Wnt8b*, and *Axin2* in *Nf2*$^{F/F}$*;Emx1-Cre* midline at E12.5 and E15.5. The *Wnt8b*$^{+}$ region is elongated dorsoventrally in E15.5 *Nf2*$^{F/F}$*;Emx1-Cre* midline (L′). Scale bars: 200 μm.

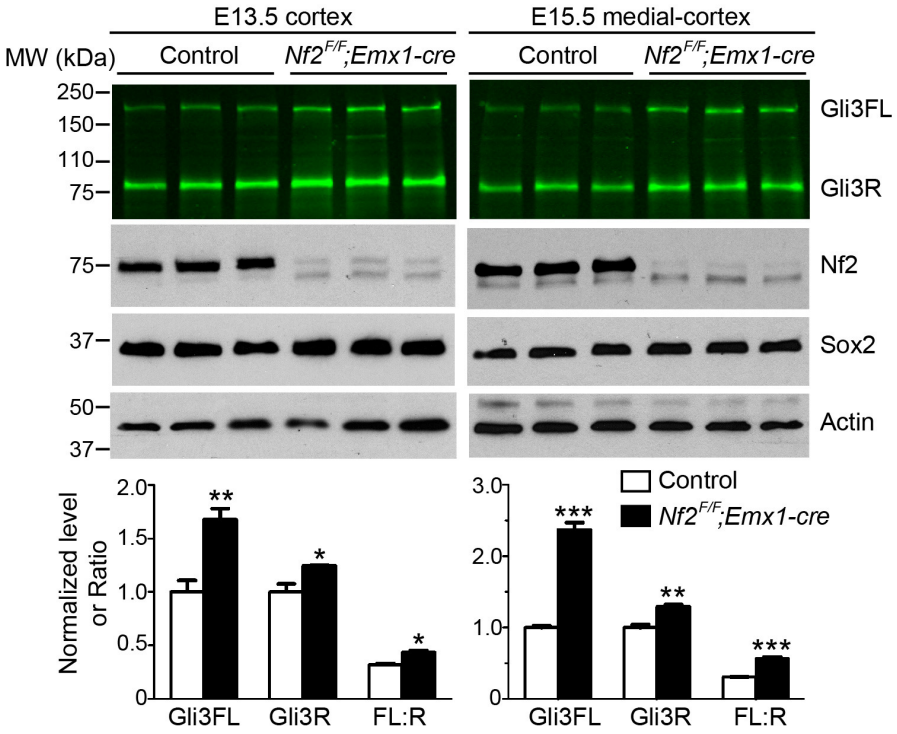

Fig. S5. Gli3 protein levels are altered in *Nf2* mutants. Quantitative western blot analyses using an antibody against the N-terminus of Gli3 detect both the full-length activator form (Gli3FL) and cleaved repressor form (Gli3R). Graphs show normalized levels of Gli3FL and Gli3R, with the levels of each form in controls set as 1, and the ratio of Gli3FL to Gli3R (FL:R). n=3 embryos per genotype, *P<0.05, **P<0.01, ***P<0.001. Because Gli3 expression is mostly restricted to neural progenitor cells, the neural progenitor marker Sox2 was used as a loading-control in addition to Actin.

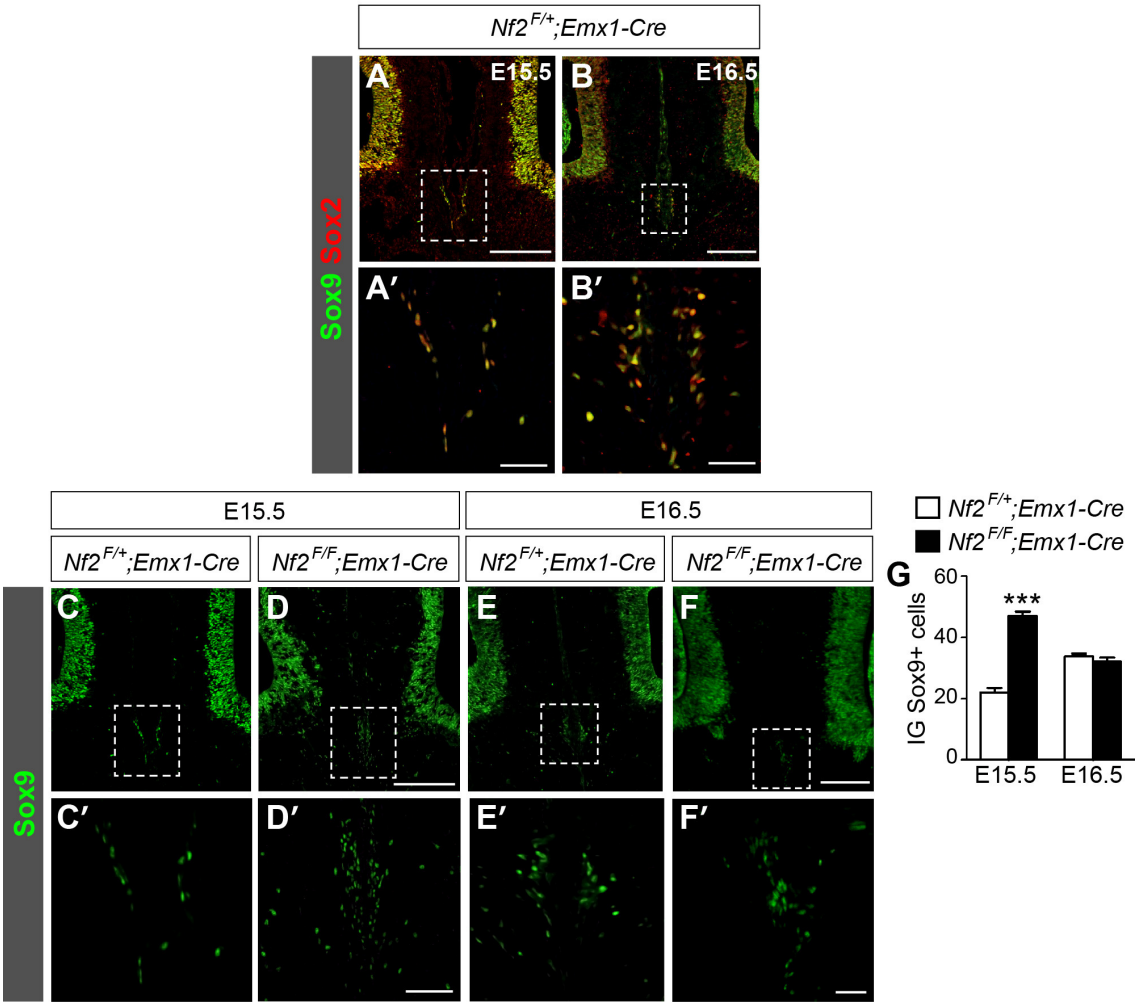

Fig. S6. The number of indusium griseum glia is transiently increased in *Nf2* mutants. (**A–C**) Co-immunostaining shows the Sox2 antibody and Sox9 antibody label the same population of cells at the indusium griseum. (**C–G**) The number of indusium griseum (IG) Sox9^{+} cells is increased in *Nf2$^{F/F}$;Emx1-Cre* embryos at E15.5 (*n*=4) but is similar to that in controls at E16.5 (*n*=3). ***P<0.001. Scale bars: 200 μm in A,B,D,F; 50 μm in A′,B′,D′; 20 μm in F′.

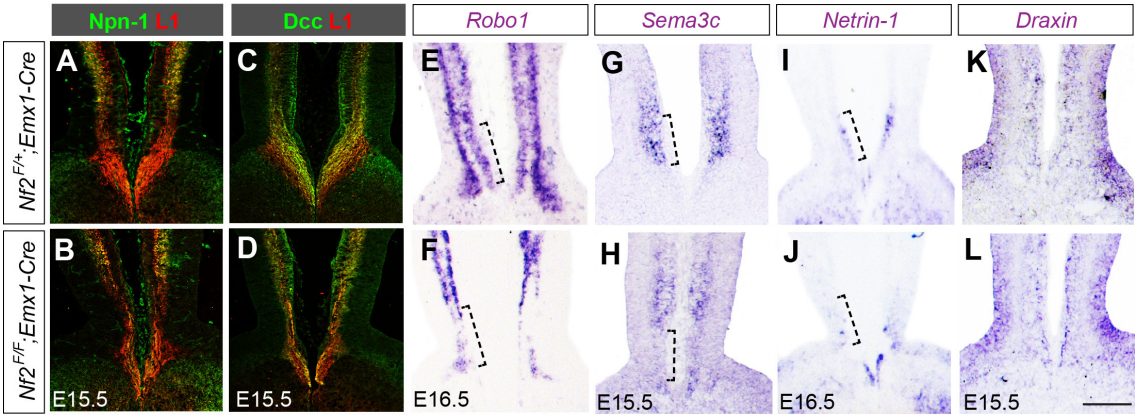

Fig. S7. Proper expression of axon guidance molecules in *Nf2* mutants. Expression patterns of guidance receptors Neuropilin-1(Npn-1), Dcc, and Robo1 and guidance cues Sema3c, Netrin-1, and Draxin are normal in *Nf2*$^{F/F}$*;Emx1-Cre* midline region. The apparent reduction of *Robo1*, *Sema3c*, and *Netrin-1 in situ* signals (dashed brackets) in *Nf2*$^{F/F}$*;Emx1-Cre* midline is likely due to reduction of the Calretinin^{+} guidepost neurons that express these genes. Scale bar: 200 μm.

Fig S8 Lavado et al.

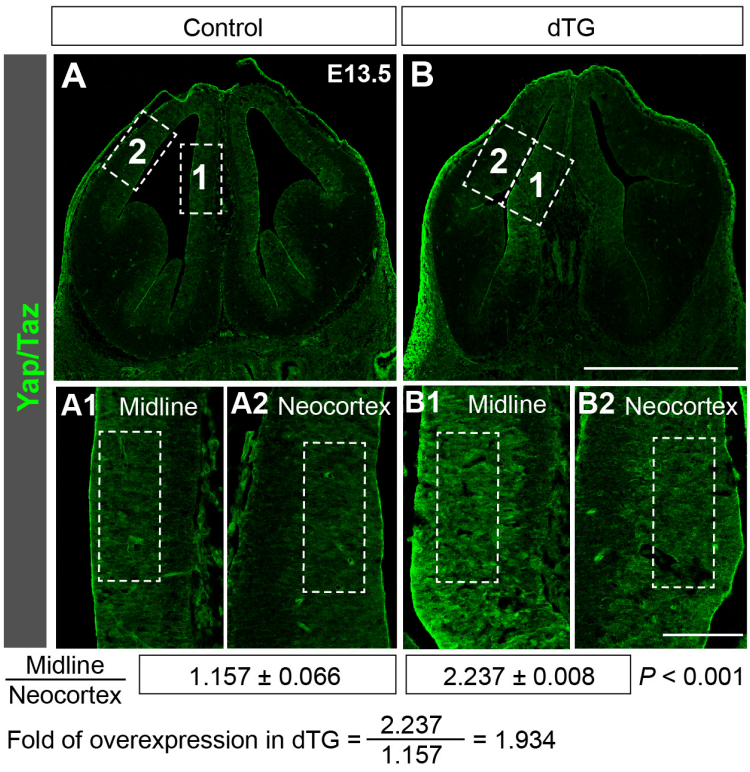

Fig. S8. Overexpressing YAP using *TetO-YAP1* and *Axin2-rtTA* double transgenic system. (**A**,**B**) Quantification of the level of YAP overexpression by measuring the fluorescence intensity of Yap/Taz immunostaining signals. To control for staining variations between sections, the intensity at the midline region (dashed box 1) was normalized to that at the neocortex region (dashed box 2) of the same section. The ratio of fluorescence intensity at the midline region and the neocortex region is shown below the confocal images. *n*=3 embryos per genotype, 6 sections per embryo. Scale bars: 1mm in B; 200 μm in B2. (**C**) Quantitative western blot analysis of E16.5 medial-cortex tissues.

Table S1. Primary antibodies for immunostaining and western blotting.

Antibody	Host species	Vendor	Catalog #	Dilution in immunostaining	Dilution in western blot
Merlin/Nf2	rabbit	Santa Cruz	sc-332	1:200 and amplification with Invitrogen TSA kit	
Nf2	rabbit	Sigma	HPA003097	1:500	1:1000
L1	rat	Millipore	MAB5272	1:500	
GFAP	rabbit	Dako	Z0334	1:1000	
Satb2	mouse	Abcam	ab51502	1:100	
Ctip2	rat	Abcam	ab18465	1:250	
Tbr1	rabbit	Abcam	ab31490	1:200	
Tbr1	rabbit	Millipore	AB10554	1:500	
Sox2	goat	Santa Cruz	sc-17320	1:100	
Sox2	rabbit	Cell Signaling	3728		1:500
Sox9	rabbit	Millipore	ab5535	1:500	
BrdU	rat	Accurate	OBT00306	1:1000	
Calretinin	rabbit	Thermo	RB-9002-P0	1:500	
Calretinin	rabbit	Millipore	AB149	1:5000	
Npn-1	goat	R&D	AF566	1:500	
Dcc	mouse	BD Pharmigen	554223	1:100	
Gli3	goat	R&D	AF3690	1:100	1:500 (ECL); 1:25 (LI-COR)
Zic2	rabbit	Millipore	AB15392	1:1000	
Tbr2	rat	eBiosciences	14-4875-82	1:500	
Tbr2 (Alexa-647-conjugated)	mouse	eBiosciences	51-4875-80	1:100	
Nf1-A	rabbit	Active motif	39398	1:1000	
Yap/Taz	rabbit	Cell Signaling	8418	1:500	
Yap	mouse	Sigma	WH0010413 M1		1:1000 (ECL); 1:100 (LI-COR)
Six3	rabbit	from G. Oliver		1:500	
GFP	chick	Aves	GFP-1020	1:1000	
Actin	mouse	Ambion	AM4302		1:40000 (ECL); 1:2000 (LI-COR)

Table S2. In situ probes

Probe	Sequence	Starts	Size (bp)
Slit2	Starts in position 4340 of rat Slit2 (NM_022632.2)	5’-TTACGTAGGAGGTATGCCTG	1600
Robo-1	Starts in position 250 of rat Robo-1 (NM_022188.1)	5’-CCCGCCACCCTCAACTGTAA	1000
Netrin-1	Starts in position 4264 of mouse Netrin-1 (NM_008744.2)	5’-TGTAGCAAATAACATCCAGC	760
Sema3C	Starts in position 1671 of mouse Sema3C (NM-013657.5)	5’-AGCAACAGTTGTACGTGAGC	700
Draxin	Full cDNA, mouse (IMAGE clone 6853328)	5’-GAGCAGCCTCCTGCCACCCG	5161
Fgf8	Full cDNA of transcript variant 4, with partials 5’-UTR and 3’-UTR, mouse (NM_001166363.1)	5’-CCCGCTCCGCGCTGAGCTGC	800
Sprouty1	Full cDNA, mouse (Addgene 22091)	5’-CCGCAGCCAGAGCTCTGCGG	1500
Wnt8b	Full cDNA, mouse (IMAGE clone 615408 moved into pCMV-SPORT2)	5’-TTCATTTCACCACCCCTTAA	478
Axin2	Starts in position 350 of mouse Axin2 (NM_015732.4)	5’-ATGAGTAGCGCCGTGTTAGT	2322

Table S3. Quantitative RT-PCR primers

Primer	Sequence	Note
mouse Axin2 forward	AAGTGTCTCTACCTCATTTTCCG	
mouse Axin2 reverse	TCCAGTTTCAGTTTCTCCAGC	
mouse Slit2 forward	GATCTCTTTAACCCCTGCCAG	
mouse Slit2 reverse	TCCCTTATCCGTTCCCCTC	
mouse Gusb forward	CACCCCTACCACTTACATCG	normalizer
mouse Gusb reverse	ACTTTGCCACCCTCATCC	normalizer
human SLIT2 forward	TCTGTTTAACCCATGCCAGG	
human SLIT2 reverse	TCTCTTATCCTTTCCCCTCGAC	
human WNT5A forward	TCGCCCAGGTTGTAATTGAAG	
human WNT5A reverse	TGAGAAAGTCCTGCCAGTTG	
human CYR61 forward	CAAGGAGCTGGGATTCGATG	
human CYR61 reverse	AAAGGGTTGTATAGGATGCGAG	
human GUSB forward	AGGTGATGGAAGAAGTGGTG	normalizer
human GUSB reverse	AGGATTTGGTGTGAGCGATC	normalizer